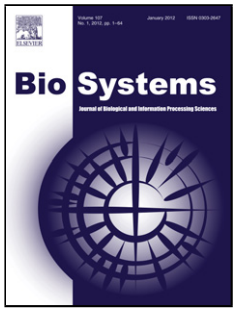

Title: LOCAL AND GLOBAL DYNAMICS IN COLLECTIVE MOVEMENTS OF EMBRYONIC CELLS

Authors: L.V. Beloussov, T.G. Troshina, N.S. Glagoleva, S.V. Kremnyov

PII: S0303-2647(18)30318-6
DOI: https://doi.org/10.1016/j.biosystems.2018.09.011
Reference: BIO 3885

To appear in: *BioSystems*

Received date: 24-8-2018
Revised date: 20-9-2018
Accepted date: 21-9-2018

Please cite this article as: Beloussov LV, Troshina TG, Glagoleva NS, Kremnyov SV, LOCAL AND GLOBAL DYNAMICS IN COLLECTIVE MOVEMENTS OF EMBRYONIC CELLS, *BioSystems* (2018), https://doi.org/10.1016/j.biosystems.2018.09.011

LOCAL AND GLOBAL DYNAMICS IN COLLECTIVE MOVEMENTS OF EMBRYONIC CELLS

L.V. Beloussov, T.G. Troshina, N.S. Glagoleva and S.V. Kremnyov*

Laboratory of Developmental Biophysics

Faculty of Biology

Lomonosov Moscow State University

Moscow 119991 Russia

*Corresponding author

E-mail s.kremnyov@gmail.com

Key words: Morphogenesis, Collective cell movements, Local order, Global order, Self-organization

Abstract

Several important morphogenetic processes belong to the category of collective cell movements (CCM), by which we mean coordinated rearrangements of many neighboring cells. The causes of the dynamic order established during CCM are still unclear. We performed statistical studies of rates and angular orientations of cell rearrangements in two kinds of embryonic tissues, which we categorized as "committed" (in the sense of being capable of autonomous CCM) as opposed to "naïve" tissues, which are those that require external forces in order to exhibit full scale CCM. In addition, we distinguished two types of cell rearrangements: first, those in which mutual cell-cell shifts characterizing the local dynamics (LD); and, second, those which moved in reference to common external coordinates (global dynamics, GD). We observed that in most cases LD rates deviated from normal distributions and do so by creating excesses of extensively converging and moderately diverging cells. In contrast, GD was characterized by nearly random behavior of slowly moving cells, combined with increased angular focusing of the fast cells trajectories as well as bimodal distribution of cell rates. When committed tissues were opposed by external mechanical forces, then they tended to preserve the inherent CCM patterns. On the other hand, the naïve ones reacted by creating two orthogonal cells flows, one of these coinciding with the force direction. We consider CCM as a self-organizing process based on feedbacks between converging and diverging cell shifts, which is able to focus the trajectories imposed by external forces.

Introduction

Several of the most important categories of morphogenetic processes that occur in development of Metazoan embryos are associated with so-called collective cell movements (CCM), in the sense of large coordinated sets of short-range deformations and rearrangements of neighboring cells. These lead to pronounced changes in macromorphology. Two main categories of CCM can be distinguished. In the first of these categories belongs the so-called contact cell polarization (Johnson, 1981; Belintzev et al. 1987), which segregate initially homogeneous epithelial layers into continuous domains of extensively columnarized and flattened cells. The second category is exemplified by mutually orthogonal convergent-extension cell movements. These produce Poisson-like two-dimensional deformations of large embryonic regions, and even of entire embryonic bodies.

Both kinds of CCM are most extensively expressed in vertebrate embryos. The first of them participates in formation of the neural plate and sensory organs, while the second one is crucial for establishing the main antero-posterior axis of embryo body (Keller and Tibbets, 1989; Keller et al., 2000). CCM also participate in morphogenesis of other taxonomic groups, such as Echinodermata (Hardin and Cheng, 1986), insects (Lecuit and Le Goff, 2007), Nematodes (Chisholm and Hardin, 2005) and to some extent hydroid polyps (Kraus, 2006). Although usually able to proceed independently from each other, in some important cases both kinds of CCM are coupled together: for example, the latero-medial cells convergence-extension in vertebrate embryos is preceded by formation of a domain of columnar cells in the immediate vicinity of the blastopore. Collective cell migrations are also important parts of regeneration and malignant growth, in both these cases demonstrating quite obvious “supracellular” properties (Friedl and Gilmour, 2009).

Within the last few decades, the behavior of individual cells (Keller and Tibbetts, 1989; Keller et al., 2000; Shih and Keller, 1992), signaling pathways (Djiane et al., 2000; Kuhl et al., 2001; Choi et al., 2002; Marsden and DeSimone, 2003; Kinoshita et al., 2003; Davidson et al., 2006; Wallingford et al., 2001, 2002) and patterns of genes expression (Darken et al., 2002; Goto and Keller, 2002) involved in CCM, and especially in convergent-extension movements have been extensively studied. Blanchard et al. (2009) performed detailed measurements of cell domains deformations in terms of individual cells motions. Meanwhile, the factors that provide holistic coordination of CCM (their positioning and orientation within embryonic bodies) are far from being clear. On one hand, CCM are susceptible to the action of external forces: as shown elsewhere (Beloussov et al., 2006; Kornikova et al., 2009), the latero-medial convergence of suprablastoporal cells of amphibian embryos is suppressed by mechanical relaxation of this tissue region. On the other hand, convergent-extension cell movements may be mechanically triggered and oriented along the stretch direction in explants of early gastrula ventral ectoderm (Beloussov

et al., 2000; Troshina et al., 2011), although these do not exhibit such movements during normal development. Importantly, CCM show the properties of self-organizing behavior. In a most straightforward manner, this is evidenced by a lack of coordinated movements in the aggregates of dissociated cells or small cell clusters which in large collectives are able to create well ordered structures (Ninomiya and Winklbauer, 2008). Also, CCM are used by developing organisms for performing certain fundamental symmetry breaks. For example, contact cell polarization breaks the translational symmetry of epithelial layers. Another example is that convergence-extension is the main tool for breaking a rotational symmetry of early embryonic bodies, thereby creating the main antero-posterior axis.

These CCM properties permit us to suggest the existence of essentially non-linear cellular and supracellular dynamics, which may be more universal that the underlain molecular events (see in this respect Zeeman, 1972). In this paper, we attempt to characterize and measure this upper level dynamics, at least a rough approximation. For this purpose, we consider separately two dynamic components: first, a set of the mutual shifts of arbitrarily selected cells (which we defined as a local component), and second, cell shifts referred to common immobile coordinates (the global component).

For such measurements, we used two kinds of embryonic tissues, both belonging to early gastrula amphibian embryos: explants of ventral ectoderm, and explants of the suprablastoporal area (SBA). In relation to CCM, this first category of samples can be defined as naïve, because (as mentioned before) they are unable to CCM. On the other hand, SBA tissues (which we define as committed) are strongly biased towards latero-medial convergence and antero-posterior extension (in relation to entire embryo coordinates) due molecular prepatterning of this area in early development. Therefore, SBA resist any forces acting in other directions. Our goal was to compare these two kinds of dynamics.

In brief, the results reported in this paper are the following. What we defined as local dynamics (LD) turned out to be essentially similar in both kinds of samples, and most clearly expressed when compared with normal distribution of the mutual cell rearrangements rates presented in a statistically detrended view. With the remarkable exception of the newly stretched tissues, all samples in the LD category were characterized by a bimodal excess of extensively converged and moderately diverged cells. The universal properties of the global dynamics (GD) were the segregation of cell movements into slow and randomly oriented on one hand, and fast/perfectly focused on the other. The naïve tissues, contrary to committed ones, responded to stretching forces by converting from fluctuated, short-termed alignment of cell shifts, to stable orthogonal cell flows. One such flow was consistently oriented along the direction of the imposed force, while the other was perpendicular to this. We discuss what kinds of mechanically-based feedbacks can

be responsible for the observed dynamics, acting within the populations of cooperatively moving cells.

Materials and methods

Xenopus laevis (Daudin) embryos obtained from hormonally stimulated adults and incubated at room temperature were used in this study.

Preparation and deformations of explants.

For preparing the double blastocoel roof explants (BRe) or suprablastoporal area explants (SBAe) the rectangular 900x900 μm pieces of embryonic ectoderm were extirpated without underlying tissues from the corresponding regions of the early gastrula (stage 10 by Nieuwkoop & Faber, 1956) *X. laevis* embryos (Fig. 1A_1, A_2), fused with each other by their internal surfaces and incubated in 10-fold diluted MMR solution (100 mM NaCl, 2 mM KCl, 2 mM Ca Cl_2, 1 mM Mg Cl_2, 5 mM HEPES, pH 7,4) (Ubbels et al, 1983) onto 2% agarose substrate. 1 min after start of incubation four glass needles of 40-50 μm diameters were inserted into explants for attaching them on the agarose substrate. In non-deformed explants all the needles were kept immobile (Fig. 1B). For stretching an explant two neighboring needles were shifted (Fig. 1C, arrows) in two steps, separated by 1-2 min interval. The resulted extension was 100-150% of the initial explant's length. For shrinking, two opposite needles were brought together (Fig. 1D, arrows). The amount of shrinkage did not exceed ≈ 50% of the transversal explant's diameter and was always associated with the deformation (folding) of its surface. Both kinds of deformations were oriented transversely to antero-posterior embryo axis, that is, perpendicularly to the elongation axis associated with gastrulation.

Confocal microscopy of actin-stained explants.

Explants of embryonic tissues were stained for actin by rhodamine-phalloidin ("http://www.cooperlab.wustl.edu/Methods/PhalloidinStain.html"). Confocal microscopy of stained samples (focused to the level of outer extodermal layer) was performed using Zeiss Axiovert200m LSM 510Meta, camera Zeiss AxioCam HRm.

Time-lapse filming and image processing

Time-lapse filming of explants was performed with the use of a digital microscope camera DCM130, mounted onto the binocular microscope Olympus SZX16. In deformed explants the filming started immediately after the end of mechanical manipulations and in non-deformed explants immediately after the start of incubation. Frames interval was 1 min and the total duration of filming lasted up to 2 h. The main bulk of measurements related to the first 20 min of explants'

incubation because later on cell movements considerably slowed down. Nevertheless, in several cases the tracing was extended up to 1h. In the total, cell movements were traced in 8 non-deformed, 8 stretched and 5 shrunk BRs, 10 non-deformed, 7 stretched and 7 shrunk SBAs.

To perform image processing, the Python language for Windows XP OS was used. Primary tracing of cell shifts was performed with the use of the pyramid Lucas-Kanade optical flow algorithm from OpenCV library of computer vision (Tarasenko and Park, 2016).

For evaluating local dynamics, the rates (μm/min) of the distances changes between arbitrarily selected pairs of cells belonging to the same explant were measured. They were defined as V_m-s, the rates of the mutual cell shifts. The initial distances between the selected cell pairs were from 3 to 5 cells diameters (70 - 115 μm). The mutual cell shifts leading to the increase of the distance between the measured cells were considered as positive, and therefore defined as diverging, while those decreasing cell-cell distances were defined as negative (in the sense of converging). We also measured the angles between the individual cells trajectories, within a range of $0 – 180^0$ (Fig. 2A-D). In these separate sets of measurements we have measured V_m-s oriented within $\pm 30^0$ angular sectors around the directions of stretching.

Evaluations of global dynamics were based upon measurements of absolute rates of cell shifts and angles of trajectories in relation to immobile rectangular coordinates. The axes of deformations were equated to $0\text{-}180^0$, zero pointed towards the shifted needle(s). So far as the deformations were always oriented perpendicularly to the embryo's antero-posterior (AP) embryo axis, this corresponded to the $90\text{-}270^0$ direction, with 270^0 being the direction pointing most directly toward the posterior embryo pole (dorsal blastoporal lip). The absolute rates of cell shifts were defined as V_d (rates of directed shifts).

A minimum of several hundred V_m-s and V_d -s measurements were performed for each experiment (see Results).

Presentation and statistical evaluations of the data obtained.

To get an overall view of the time-lapse data, vector maps of cell shifts were constructed. The next step was to present V_d and V_m values in polar coordinates covering in first case $0\text{-}360^0$ and in the second case $0\text{-}180^0$. Statistical significance of differences between linear and angular V_d and V_m values were determined, using Pearson correlation coefficients between V_d values. Positions along the x axis and their angular density were estimated using the «STATISTICA 6.0» program, section “Basic Statistics”. Empirical distributions of linear V_d and V_m values were evaluate for their normality, with the use of Lilliefors criteria and presented in detrended form.

Long-range order in cell shifts was evaluated with the use of the order parameter S (applied to cell orientations by Pietak and Waldman, 2008) calculated as

$$S = \frac{\langle 3(\cos\varphi)^2 - 1 \rangle}{2}$$

where φ was the angle between the orientation of a given cell trajectory and an arbitrary axis of an immobile coordinate system (for example, the axis of stretching) and the numerator $<3(\cos\varphi)^2 - 1>$ was the average of a set of functions $[3(\cos\varphi)^2 - 1]$ calculated for all the cells trajectories belonging to a single sample or to a selected group of similar samples. The maximal orientation order corresponds to S= +1, and the maximal deviation from the ordered state (all the cells trajectories are oriented perpendicularly to each other or the given axis) is S = – ½. In several cases the results were presented as histograms of the functions $[3(\cos\varphi)^2 - 1]$ divided into columns with φ values binned at 15^0.

Results

Changes in morphology and cell structure of explants as traced by time lapse filming and confocal histology.

The following features of the overall morphology of both stretched and non-stretched explants are of importance: (1) condensations of ectodermal cells along the stretch direction (as traced by pigmentation patterns) can be noticed immediately after the end of stretching (Fig. 3A). Hence, the condensations can be ascribed to the *passive* ("Poissonian") shrinkage in the axis perpendicular to the stretching force or, alternatively, the condensation could follow from the "durotaxis" (see Evstifeeva et al., 2018). (2) On the other hand, within several hours after the end of deformations, the polar tissue regions considerably overlapped the stretching needles (Fig. 3C, encircled areas). This indicates the *active* extension of a sample proceeding in the direction of previous stretching. (3) As shown by time lapse, a surface of non-stretched explants was in a state of permanent oscillation. As a result, transitory grooves emerged, most of them oriented roughly orthogonal to each other (Fig. 3D inset, dashed lines).

As shown by confocal views of actin-stained samples, at the start of incubation the outer ectodermal layer consisted of quite uniform, roughly isodiametric cells (Fig. 3D). Subsequent evolution of non-stretched explants was characterized by the appearance of a few isolated, tangentially contracted cells (Fig. 3E, arrow) and formation of aligned cell files (Fig. 3E). (For statistical evaluation of cell shape changes see Evstifeeva et al., this issue. Regarding the stretched explants (Fig. 3F-H), one should note first of all that immediately after the end of stretching the individual cells were deformed only slightly (Fig. 3F), and the main elongation in

the stretch direction took place within less than 10 min after the cessation of stretching. Therefore, cell elongation should be regarded as an active post-stretching event, correlated with the previously described overlapping of the polar explants regions (Fig. 3G). After the next few dozen minutes, most of cells again approached an isodiametric shape (Fig. 3H).

The main conclusion from confocal images, which is further supported by time-lapse observations, is that the outer ectodermal layer of both the intact and the experimentally perturbed samples consist of densely packed cells, which can be extensively deformed but do not undergo intercalation moments. Accordingly, what we define as the shifts (either mutual or directed) of cells A and B can in no way be identified with their free movements. Instead, they are direct consequences of contractions (in case of convergence) or extensions (in case of divergence) of cells located between A and B and are equal to algebraic sums of the contraction-promoted decrease and the extension-promoted increase along the AB line. Thus, Vm-s can be considered as an integral index of the linear tissue deformation within a given region. Chosen time interval allows us to assume tissue reaction on stretching predominantly elastic. Although prevailing elastic behavior has been reported for ultrashort timescales, i.e. several seconds (Forgacs et al., 1998, Serra-Picamal et al., 2012), time interval chosen for detecting cell shifts is not sufficient for triggering cell rearrangements that mediate fluidization of the tissue.

However, cell rearrangements (and thus possible sources of deformations) are not restricted to intercalation movements (Guillot, Lecuit, 2013). Mutual cell rearrangements must be taken into account. Yet, these types of cell movements are not always accompanied with significant displacement and hence can be an integral index only in limited cases.

Survey of the vector maps.

Vector maps of epi-ectodermal cells trajectories, covering the first 15 min of incubation, display a different set of patterns (Fig. 4). First, one can see a distinct difference between cells trajectories in non-deformed BRe and SBAe. Specifically, in BRe, they are much shorter and more chaotically arranged (Fig. 4A). In contrast to this, SBAe cells are uniformly directed towards the posterior embryo pole, thus retaining the normal blastopore-directed movements (Fig. 4C). Within the stretched BRe and SBAe, cell trajectories are more similar to each other, in that they always demonstrate cell flows along the stretch axis (Fig. 4B, D). Meanwhile, in BRe the main stretch-oriented cell flow is always accompanied by movements which bring cells towards the axis of stretching, thereby precisely simulating convergent-extension, which is peculiar to CCM involved in the formation of axial organs (Fig. 4B). In contrast, there is not much convergence towards the stretch axis by transversely stretched SBAe cells (this axis being in the transversal direction of the embryonic body). Instead, posteriorly directed cell flow continues to dominate (Fig. 4D). In addition, in some of SBAe we have observed complicated vortex-like cell flows (Fig. 4E). In the

shrunken BRe, cell movements between the shifted needles were slow and chaotic (not shown), while in SBAe most of cells were moving toward the posterior, in other words, perpendicularly to the direction of shrinkage (Fig. 4F).

Properties of local cell dynamics: alignment tendencies as a pathway to a global order; bimodal distributions.

As seen from Table 1, the average rates of the divergent and convergent V_m–s take the smallest and approximately equal values in non-stretched and shrunk BRe samples, as well as in the intact (non-explanted) SBA. Therefore, in all these cases, the average density of cell arrangement remains roughly constant during the entire observation period. In contrast, in the newly stretched BRe, and in all the varieties of SBAe, the average diverging rates significantly exceed the converging ones; this indicates the domination of cell extension over contraction.

Among the both deformed and non-deformed samples, the average angles α between cells trajectories (both divergent and convergent) did not exceed ≈ 20^0 (Table 1; Fig. 5), fitting the patterns shown in Fig. 2, A, B. Accordingly, most of cells tend to align their trajectories and shift in the same direction. The alignment and uni-directionality were the greatest in the intact SBA (trajectories of the mutual cell shifts almost parallel). Among the experimental samples, this was most of all pronounced in stretched BRe and transversely shrunk SBA (Fig. 5, cf B and A, C; F and D, E).

At the same time, as seen from Fig. 5, some small fraction of cell trajectories (no more than a few percent) were oriented to each other at $\alpha>90^0$, in other words directed to the opposite sides (as those depicted in Fig. 2 C, D). Thus, one can assume that all the samples consist of the domains populated by cells shifted in the same direction along the aligned trajectories ($\alpha << 90^0$) and separated from each other by narrow bands (separatrices) demarcating the oppositely directed cell flows. Therefore, the ratios R of the trajectories pairs with $\alpha>90^0$ to those with $\alpha<90^0$ are roughly equal to the ratios between the squares of zones having properties of separatrices and the squares of the domains occupied by uniformly directed cell flows. So far as separatrices should be in many orders thinner than the domains (as confirmed by figures given in frames A-F, Fig.5), their “squares” should be reduced to lengths. Under these conditions, R values give a measure of tortuosity of the domains borders which may be considered as being reverse to what we would define as a simplicity, or global order of the domains' structure.

By R criteria, BRe and SBAe behave in almost the reverse ways. Among stretched BRe, the R value was two times smaller than in non-stretched samples (Fig. 5, cf. A and B). Therefore, in this case, the stretching simplifies the domains structure. On the other hand, R value for shrunk samples were the highest (Fig. 5C). Meanwhile, among SBAe, both stretched and non-stretched samples had roughly equal (and relatively high) R values (Fig. 5, cf. D and E), while the shrunk

samples have R values about an order smaller (Fig. 5F). Accordingly, in this case it was the shrinkage rather than stretching which simplified the domain structure, and thus increased the global order. We explain this by pointing to the inherent deforming tendencies of SBAe (lacking in Bre). Specifically, in the SBAe cases, the transversal stretching was directed against the natural tendency of this area to contract transversely, and the longitudinal shrinkage is in tune with these.

These conclusions are visualized by 2-dimensional mapping of cell movement rates in individual representatives of different series (Fig. 6A-D). While the domain's structure of non-stretched BRe was relatively complicated and irregular, with prolonged tortuous separatrices (Fig. 6A, B), it was greatly simplified by stretching, being reducing to a single axi-symmetric domain (Fig. 6 C-F). Meanwhile, in transversely stretched SBAe the complicated domains structure remained unaffected (Fig. 6I, K) in comparison to that of BRe.

Another V_m-s feature which we consider to be most important was their relation to normal distributions. While looking at first glance similar to normal ones, in fact none of Vm-s distributions satisfied Lilliefors criteria (Lilliefors, 1967). More detailed study of detrended the empirical distributions showed that at the start of incubation they were more or less close to normal but later on, with different rates, approached towards a bimodal state characterized by two overnormal excesses, the left of these corresponding to a relatively small fraction of extensively converging (contracted) cells while the right one corresponds to a greater fraction of moderately diverging (extended) ones (Figs. 7, 8). The rate of approaching towards bimodality largely depended upon mechanical regimes, especially in BRe cases: in these samples the stretching extensively retarded the approach to bimodality (Fig. 7B-J), while in shrunk explants this transition took a few minutes (Fig. 7C, F) and non-stretched explants were characterized by intermediate rates (Fig. 7A-I). Mechanically, SBAe were much less affected, but kept the same tendencies (Fig. 8 A-F). Notably, the intact (non-isolated) SBA also exhibited a bimodal pattern, although the both modes were much closer to a zero value (Fig. 8G).

Individual V_m –s distributions were quite variable but kept nevertheless in most cases the over-normal excesses of extreme values (Fig. 9). In other words, the cells were segregated to those extensively approaching and shifted apart from each other. Obviously, within the dense populations of strongly adhered cells this will lead to increase of tensions (see Discussion, Evstifeeva et al., 2018) .

Temporal V_m–s dynamics for aligned cell shifts: contraction-extension “swings”

The average rates within BRe sets of converging-divergent mutual cell shifts oriented along the directions of stretching and the corresponding directions of non-stretched samples were measured for two successive time periods (0-5 min and 5-15 min after start of incubation). During the first period, the average rates of cell divergence exceeded those of cell convergence (the

difference was mostly obvious for stretched samples). In the second period, the reverse took place (Fig. 10A, B). These data will be relevant for a subsequent discussion.

Properties of the global dynamics: patterns of cell flows, rate-dependent ordering, bimodality appearing again

Fluctuating cell flows in non-stretched BRe and stable orthogonal flows in stretched samples. As seen from Fig. 11, the *directed* cell shifts (V_d) in non-stretched BRe are located each during each time interval of several minutes, within a rather narrow angular range, they drastically change their orientation relative to the next time interval. Also, the dominating orientations of the individual samples trajectories are quite different in relation to any external coordinate grid. Accordingly, when calculating the order parameter (S) value for the entire V_d set of non-stretched BRe, we get for the first 15 min of incubation a rather low value (S_1=0,13±0,11). Meanwhile, if we match each subsequent individual sample's main coordinates axis with the orientation of its dominating cell flow, we get for the same time interval a much higher value (S_2=0,46±0,29). The difference $\Delta = S_2 - S_1$ can be taken as a measure of the *individual fluctuating alignment* of cell trajectories: the greater it is, the more focused is each individual bundle of trajectories and the less definite is its orientation according to any common coordinate system.

Another method for evaluating the directed cell flows is to construct histograms of nominators [3 (cosφ)2 – 1] of the order parameter calculated for each 8^0 interval separately within a 0-90^0 range (see Materials and Methods). The left column of Fig. 12 displays such data for the set of matched non-stretched BRe. One can see that during the first 15 min of incubation the dominating flows are accompanied by perpendicular ones, although the latter are much smaller and soon disappear. At the same time, the dominating ones are also gradually reduced. This is in sharp contrast with the similar patterns in stretched BRe (Fig. 12, middle and right columns).

They are characterized by a prolonged maintenance of two mutually perpendicular flows, one of them (the right one) coinciding with stretch direction. The latter is more or less constant during the entire observation period, while the intensity of the perpendicular one fluctuates.

Another important property of both the orthogonal flows which can be seen in 2-dimensional maps (Fig. 6 C-F) is that the rates of latero-medial cell movements are increased towards the explant's periphery in a linear fashion. The same is true for the longitudinal movements along the explants' midlines, as traced from one sample’s pole towards the opposite pole. We discuss these data in the next section.

With regard to SBAe, one should notice first of all the preservation of both the orthogonal cell flows (taking place during normal development) in non-stretched samples (Fig. 13A). The transversal SBAe stretching led to a short-termed domination of stretch-oriented flow (Fig. 13B),

while transversal shrinkage to the domination of antero-posterior one, that is oriented perpendicularly to the applied force (Fig. 13C). In general, by a criteria of V_d dynamics (as well as by that of V_m dynamics, see Fig. 8 and the corresponding comments) SBAe samples showed much greater structural stability than BRe.

Rate-dependent angular focusing and positive correlations between cell rates and the angular densities of cells trajectories. As illustrated by the rates/angles V_d diagrams (Figs 14, 15), both BRe and SBAe cells can be divided into two categories: (1) those moving slowly (rates non-exceeding ≈ 2μm/min) and more or less equally in all directions, and (2) faster ones, their trajectories located within narrow sectors and focused proportionally to their rates (Fig. 14B, C; 15A-D, F). As seen from Fig. 14, among BRe such sharpened “protuberances” take place only in stretched samples and are adjusted to $0/360^0$ (that is to the direction of force application) while perpendicular cell flows are slower and smoothed. On the contrary, among non-stretched and shrunk SBAe well pronounced protuberances are maintained during the whole time of the observations (Fig. 15 A, D, C, F) while in the stretched samples they disappear in a few minutes after the start of incubation (Fig. 15 cf B and E). The orientation of stable protuberances (about 270^0) precisely coincides with that of the blastopore-directed cell flows of the intact embryos (Fig. 15D, inset), while the orientation of unstable protuberances in stretched SBA deviates from this direction by $70\text{-}80^0$. Thus, in SBAe samples, contrary to BRe, a coincidence of cell flows' orientation with that taking place in normal development is crucial for their stability.

Another manifestation of a rate-dependent focusing is a strict positive correlation between the number of cells moving within a given angular sector and their average rate, and this occurred in all categories of samples (Table 2).

Slow and fast cells have discrete characteristic rates (see also Evstifeeva et al., 2018). In most of samples with well-expressed fast cell fractions (except 5 min stretched BRe and shrunk SBA) the distributions of the directed cell movement rates were definitely bimodal, the left peak corresponding to a slow fraction (2-4 μm/min) while the right (in most cases marginal) one to fast cells (Fig. 16). Under more detailed observations some additional peaks within the slow fraction (most expressed in non-stretched and intact SBAe) can be seen. This indicates not only the presence of the inherent differences between both cell fractions, but also a general tendency of cell movement rates, including those belonging to intact embryos, to take discrete values.

Discussion

The main aim of this study was to explore whether collective movements of embryonic cells can be associated with some kind of universal dynamics expressed on a cellular/supracellular level. In searching for such a dynamics, we used two reference systems: a local or a relational one measuring individual cell shifts irrespective of their positions within a whole explant, and a global

system describing all cell shifts within a given sample as well as any external forces which may act upon them with the use of a common coordinate system. Now our aim will be to embrace both these kinds of dynamics by a common model.

Local dynamics: morphogenetic role and a possible mechanical basis. As described before (see Figs 7, 8 and the corresponding comments), the most universal feature of the local dynamics is a tendency to produce bimodal patterns consisting of few extensively converged (tangentially contracted) and a greater amount of moderately diverged (tangentially extended) cells; in addition, most of the local shift trajectories are aligned in definite directions. With the exception of intact samples (where no temporal dynamics can be traced due to the presence of one time point only) these patterns are not stationary but are gradually evolving from the states characterized by quasi-normal distributions towards a pronounced bimodality. This permits us to regard bimodal states as universal dynamic attractors to which cell populations are driven after initial perturbations (isolation, mechanical deformations). This drive is most obvious in the case of BRe, but it can be traced also in SBAe in spite of their greater resistance to the experimental perturbations. We find it notable that any external perturbation (and most of all a directed stretching of BRe) instead of reducing a symmetry order and bringing cell populations towards the less probable state, instead has the opposite effect, essentially simplifying the explants' structure (see Fig. 6, cf. A, B and C, D); at the same time, a progressive loss of symmetry (segregation of a unimodal and spatially homogeneous cell structure towards two alternative states (see Fig. 3 cf D and E) occurs spontaneously. This may take place only in far-from-equilibrium systems and emphasizes a role of non-equilibrium phenomena in the observed dynamics.

The bimodal dynamics is in no way exotic: it is easy to see that it is directed towards producing spatially restricted domains of tangentially contracted (and hence columnar) cells connected by prolonged files of moderately extended (flattened) ones. This is just what is taking place during formation of a domain of bottle-shaped cells in the vicinity of the blastopore, neural plate, sensory placodes, etc. Note also that segregation of initially homogeneous cell layers into columnar and flattened cell domains should be associated with increase of tensions produced by contracted cells and transmitted by extended ones.

What might be the basis of such a dynamics? Its spontaneity implies the existence of a positive feedback between the contraction and extension of mechanically coupled cells. Such a feedback is indeed expected within a framework of the hyper-restoration (HR) model of morphogenesis (Beloussov, 2008, 2012). By this model, a tendency to over-compensate any deviation from a mechanical homeostasis should lead to a gradual segregation of an initially homogeneous cell mass into the domains of tangentially contracted (columnar) and extended (flattened) cells (Fig. 17A-C). Similar alternation of the regions of predominantly tensile and compressive stresses are

taking place in cell monolayers (Tambe et al., 2011). The model predicts also that the domains should be arranged, at least at the time of their formation, along straight lines, assuming that the feedback is mediated by pressure and tension forces exerted by these domains. Another expectation of the model is that (due to overshoots), the rates of contraction and extension should fluctuate periodically overlapping one another.

Both these expectations are indeed confirmed: an overwhelming majority of both divergent and convergent mutual cell shifts are almost parallel to each other (Table 1; Fig. 7) and as shown by Fig. 10, they act in a swing-like manner, alternating with each other.

In what way is it possible to explain the effects of different mechanical regimes upon the rate of such a drive towards bimodality? Most probably, the retarding effect of stretching is in delaying the formation of tangentially contracted cells and thus preventing the closure of a feedback loop. Based on direct observations (Fig. 3G) and in accordance with HR model (Fig. 17A) such cells can be formed in the stretched samples only after most of other cells have been *actively* extended in the stretch direction thus transforming a longitudinal stretching into a similarly directed pressure. Under these circumstances, cell contraction should dominate over extension (as shown in Fig. 10B) so that the reverse step of a contraction-extension feedback loop could come into action.

On the other hand, shrinkage of explants creates a unique situation when the external mechanics itself (probably even without involving active feedbacks) is enough for facilitating both cell contraction (in the direction of a compressing force) and cell extension (perpendicularly to this force). This may explain an extremely fast (taking no more than about 5 min) establishment of a bimodality followed by a halt of mutual cell shifts. Within such a framework it is but natural that in non-stretched samples the rate of approach towards bimodality occupies an intermediate position between these two extremes.

Dynamics of directed cell shifts: fluctuating background and self-focusing of advanced cell flows. A main property of the directed cell flows which is common for all the categories of the samples is their segregation into two fractions: the cells which move slowly (≤ 2 μm/min) in random directions and those moving faster (up to 10-12 μm/min) along precisely oriented and self-focused flows (Fig. 14, 15). (Please note that in Fig. 6 and the corresponding comments that cell rates oriented along the applied force increase in a linear fashion towards the explants' margin, indicating that each successive cell rate is actually a sum of rates of all those cells situated behind; therefore high rates of some cells are due to their arrangement rather than individual properties).

Notably, each cell fraction has its own discrete characteristic rate distinguished from that to be expected based on the presumption of a common normal distribution (Fig. 16). The rate

characterizing a slow fraction is of the same order as the rates of the mutual cell movements. In other words, these movements, while being presented within a common coordinate system, behave similarly to a random noise. We speculate that the biological role of the random noise is to scan mechanical stresses in the immediate surroundings (similarly to vibrating electrodes). It is known indeed (Harris et al., 1980) that even individual cells are permanently scanning the substrate by their micromovements and more recently similar movements qualified as a “dynamic chaos” were traced in fish embryos (Cherdantzev and Tsvetkova, 2005). Low rates and random directions of such movements are biologically suitable as they do not disturb the main tensions and permit the cells to get a “mechanical information” from all directions. It is worth mentioning that similar fluctuating “superdiffusive” shifts of membrane particles ascribed to random non-thermal forces acting within cytoskeleton have been traced (Lau et al., 2003). It would be of interest to know whether these lower level shifts are somehow connected with the above described random exploring activity of entire cells.

Coming back now to fast fractions (which best of all represent the main features of the collective cell movements), we have to explain two effects: (1) self-focusing of cell flows, which is obvious when compared with the much more smoothed external forces applied to the marginally located needles (see Fig. 1C); (2) cooperative action of longitudinal and transversal flows.

A possible scenario is based upon the integral effects of the active longitudinal extension and transversal contraction of stretched explant cells (Fig. 18). The above-mentioned summing up of the active cell extensions within several longitudinal rows will generate along its flanks the gradients of passive tensions increasing from the center to periphery (Fig. 18 A, B; tension gradients shown by shadowed double-headed arrows). In addition, this very extension will shrink the polar areas (Fig. 18B, converged blue arrows). According to the HR model, the latter deformation is expected to be transformed into active contraction (same frame, nearby located red arrows), which increases tension.

At the same time, in the transverse direction, quite similar transformations are expected, generating meanwhile a pressure gradient instead of a tensile one. Summing up of the active transversal cell contractions will stretch in the same direction the lateral zones (Fig. 18C, blue double-headed arrows), this stretching being expected to transform into active extension (same frame, red arrows). As a result, the longitudinal tension gradients will be combined with the laterally located pressure areas (Fig. 18D, blue semicircles). Based on several sets of evidence (Beloussov et al., 2000; Mansurov et al., 2012) embryonic cells tend to move uphill along tension gradients, even if they have to overcome during this movement a certain resistive force. Thus, the expected movements (cell flows) will be directed towards polar-medial areas (Fig. 18D) and hence focused.

An unexpected conclusion from our data is that the differences between two explored embryonic regions– an uncommitted blastocoel roof tissue and a suprablastoporal area with a strictly determined set of potencies – can be formulated not only at the level of molecular signaling, as it is done usually (De Robertis, 2009), but also in the terms of mechanosensitive long-range architectonics. It is indeed only the blastocoel roof tissue which can be regarded at the early gastrula stage as a tabula rasa, completely open to the actions of mechanical forces. Instead, the same stage suprablastoporal area, in spite of a considerable variability and clustering of cell movements (see Fig. 4E; 6G-K) possesses an already predetermined pattern of cell movements, so that the actions of any forces which do not coincide with it (for example, transversal stretching) produce nothing except short-termed effects which will be soon annihilated; on the other hand, those actions which are in tune with the presumptive pattern (longitudinal shrinkage) are enhanced. One may conclude that in addition to being a source of putative inductive substances, a native SBA has also properties of a mechano-geometric attractor.

Declarations

Authors' Contribution

TGT, NSG and SVK performed all experiments. LVB developed the concept, performed the data analysis, and wrote the first version of the manuscript. All authors contributed to the final version of the manuscript.

Consent for publication

All authors have approved the manuscript for submission

Competing interests

The authors declare that they have no competing interests.

Ethics approval and consent to participate

Not applicable

Acknowledgements

The authors are greatly indebted to Prof. Albert Harris for his valuable comments and checking of the manuscript. This work was supported by the Russian Fund for Fundamental Research (RFFI) grant # 14-04-00337 and by federal project AAAA-A16-116021660089-6.

References

Belintzev, B.N., Beloussov, L.V., Zaraiskii, A.G., 1987. Model of pattern formation in epithelial morphogenesis. J. Theor. Biol. 129, 369-394.

Beloussov, L.V., Luchinskaia, N.N., Stein, A.A., 2000. Tension-dependent collective cell movements in the early gastrula ectoderm of Xenopus laevis embryos. Dev. Genes and Evolution. 210, 92-104.

Beloussov, L.V., Luchinskaia, N.N., Ermakov, A.S. and Glagoleva N.S., 2006. Gastrulation in amphibian embryos, regarded as a succession of biomechanical feedback events. Int. J. Dev Biol. 50, 113-122.

Beloussov, L.V., 2012. Morphogenesis as a macroscopic self-organizing process. BioSystems. 109, 262-279.

Benazeraf, B., Francois, P., Baker, R.E., Denans, N., Little, Ch. D., Pourquie, O., 2010. A random cell motility gradient downstream of FGF controls elongation of amniote embryo. Nature. 466, 248-251.

Blanchard, G.B., Kabla, A.J., Schultz, N.L., Butler, L.C., Sanson, B., Gorfinkiel, N., Mahadevan, L. and Adams, R.J., 2009. Tissue tectonics: morphogenetic strain rates, cell shape change and intercalation. Nature Methods. 6, 458-464.

Chisholm, A.D., Hardin, J., 2005. Epidermal morphogenesis. WormBook. 1-22.

De Robertis, E.M. 2009. Spemann's organizer and the self-regulation of embryonic fields. Mech. Devel. 126, 925-941.

Cherdantzev, V.G. and Tsvetkova N.V., 2005. Dynamics and variability of the early morphogenesis in loach (Misgurnus fossilis L.) based on observations of individual developmental path. Ontogenez (Russ. J. Dev. Biol.). 41, 1-14.

Choi, S.C. and Han, J.K., 2002. Xenopus Cdc42 regulates convergent extension movements during gastrulation through Wnt/Ca(2+) signalling pathway. Dev. Biol. 244(2), 342-357.

Darken, R.S., Scola, A.M., Rakeman, A.S., Das, G., Mlodzik, M. and Wilson, P.A. 2002. The planar polarity gene strabismus regulates convergent extension movements in Xenopus. EMBO J. 21(5), 976-985.

Davidson, L.A., Marsden, M., Keller, R. and Desimone, D.W., 2006. Integrin alpha5beta1 and fibronectin regulate polarized cell protrusions required for Xenopus convergence and extension. Curr. Biol. 16(9), 833-844.

Djiane, A., Riou, J., Umbhauer, M., Boucaut, J. and Shi, D. 2000. Role of frizzled 7 in the regulation of convergent extension movements during gastrulation in Xenopus laevis. Development. 127(14). 3091-3100.

Evstifeeva, A. Iu., Kremnev, S.V., Belousov, L.V., 2010. Changes in topology and geometry of the embryonic epithelium of Xenopus during relaxation of mechanical tension. Ontogenez (Russ. J. Dev. Biol.). 41, 190-198.

Evstifeeva, A.Yu., Luchinskaia, N.N., Beloussov, L.V., 2018. Stress-generating tissue deformations in Xenopus embryos: long-range gradients and local cell displacements. this issue.

Forgacs, G., Foty, R.A., Shafrir, Y., Steinberg, M.S., 1998. Viscoelastic Properties of Living Embryonic Tissues : a Quantitative Study. Biophys. J. 74, 2227–2234.

Friedl, P., Gilmour, D., 2009. Collective cell migration in morphogenesis, regeneration and cancer. Nat. Rev. Mol. Cell. Biol. 10, 445-457.

Goto, T. and Keller, R., 2002. The planar cell polarity gene strabismus regulates convergence and extension and neural fold closure in Xenopus. Dev. Biol. 247(1), 165-181.

Guillot, C., Lecuit, T., 2013. Mechanics of epithelial tissue homeostasis and morphogenesis. Science. 2013340(6137), 1185-1189.

Hardin, J.D. and Cheng, L.Y., 1986. The mechanisms and mechanics of archenteron elongation during sea urchin gastrulation. Dev Biol. 115, 490-501.

Harris, A.K., Wild, P. and Stopak, D., 1980. Silicone rubber substrata: a new wrinkle in the study of cell locomotion. Science. 208, 177-179.

Isenberg, B. C., DiMilla, P. A., Walker, M., Kim, S., Wong, J. Y., 2009. Vascular Smooth Muscle Cell Durotaxis Depends on Substrate Stiffness Gradient Strength. Biophysic. J. 97, 1313-1322

Jenny, A., Darken, R.S., Wilson, P.A., and Mlodzik, M., 2003. Prickle and Strabismus form a functional complex to generate a correct axis during planar cell polarity signaling. EMBO J. 22(17), 4409-4420.

Johnson, M.H. 1981. Membrane events associated with the generation of a blastocyst. Int. Rev. Cytol. Suppl. 12, 1-37.

Keller, R. and Tibbetts, P. 1989. Mediolateral cell intercalation in the dorsal, axial mesoderm of Xenopus laevis. Dev. Biol. 131(2), 539-549.

Keller, R., Davidson, L., Edlund, A., Elul, T., Ezin, M., Shook, D. and Skoglund, P., 2000. Mechanisms of convergence and extension by cell intercalation. Philos. Trans. R. Soc. Lond. B. Biol. Sci. 355(1399), 897-922.

Kinoshita, N., Iioka, H., Miyakoshi, A., and Ueno, N., 2003. PKC delta is essential for Dishevelled function in a noncanonical Wnt pathway that regulates Xenopus convergent extension movements. Genes Dev., 17(13), 1663–1676.

Kornikova, E.S., Korvin-Pavlovskaya, E.G. and Beloussov, L.V., 2009. Relocations of cell convergence sites and formation of pharyngula-like shapes in mechanically relaxed Xenopus embryos. Development, Genes and Evolution. 219, 1-10.

Kraus, Ju. A. 2006. Morphomechanical programming of morphogenesis in Cnidarian embryos. Int.J.Dev.Biol. 50, 267-275.

Lau, A.W.C., Hoffman, B.D., Davies, A., Crocker, J.C. and Lubensky T.C., 2003. Microrheology, stress fluctuations and active behavior of living cells. Phys. Rev. Lett. 91, 198101.

Lecuit, T. and Goff, L. Le., 2007. Orchestrating size and shape during morphogenesis. Nature. 450. 189-192.

Kühl, M., Geis, K., Sheldahl, L.C., Pukrop, T., Moon, R.T. and Wedlich, D., 2001. Antagonistic regulation of convergent extension movements in Xenopus by Wnt/beta-catenin and Wnt/Ca2+ signaling. Mech. Dev. 106(1-2), 61-76.

Marsden, M. and DeSimone, D.W., 2003. Integrin-ECM interactions regulate cadherin-dependent cell adhesion and are required for convergent extension in Xenopus. Curr. Biol.13(14), 1182-91.

Lilliefors, H. W., 1967. On the Kolmogorov-Smirnov test for normality with mean and variance unknown. Journal of the American Statistical Association. 62, 399–402.

Ninomiya, H. and Winklbauer, R., 2008. Epithelial coating controls mesenchymal shape change through tissue-positioning effects and reduction of surface-minimizing tension. Nature Cell Biol. 10, 61-69.

Pietak, A. and Waldman, S. D., 2008. Seeing tissue as a “phase of matter”: exploring statistical mechanics for the cell. Phys. Biol. 5, 016007.

Serra-Picamal, X., Conte, V., Vincent, R., Anon, E., Tambe, D.T., Bazellieres, E., Butler, J.P., Fredberg, J.J., Trepat, X., 2012. Mechanical waves during tissue expansion. Nat. Phys. 8, 628–634.

Shih, J. and Keller, R., 1992. Cell motility driving mediolateral intercalation in explants of Xenopus laevis. Development. 116(4), 901-914.

Tambe, D.T. and 11 co-authors, 2011. Collective cell guidance by cooperative intercellular forces. Nat. Mater. 10(6), 469-475.

Tarasenko, V. and Park, D.-W., 2016. Detection and Tracking over Image Pyramids using Lucas and Kanade Algorithm. International Journal of Applied Engineering Research. 11(9), 6117-6120.

Troshina, T.G., Glagoleva, N.S., Beloussov, L.V., 2011. Statistical study of rapid mechanodependent cell movements in deformed explants in Xenopus laevis embryonic tissues. Ontogenez (Russ. J. Dev Biol), 42, 301-310.

Ubbels, G.A., Hara, K., Koster, C.H., Kirschner, M.W., 1983. Evidence for a functional role of the cytoskeleton in determination of the dorsoventral axis in Xenopus laevis eggs. J. Embryol. Exp. Morphol. 77, 15–37.

Wallingford, J.B., Ewald, A.J., Harland, R.M. and Fraser, S.E., 2001. Calcium signaling during convergent extension in Xenopus. Curr. Biol. 11(9), 652-661.

Wallingford, J.B., Fraser, S.E., Harland, R.M., 2002. Convergent extension: the molecular control of polarized cell movement during embryonic development. Dev. Cell. 2(6), 695-706.

Zeeman, E.C., 1972. Differential equations for the heartbeat and nerve impulse. Towards Theor. Biol. (C.H. Waddington ed). 4, 8-67.

Legends:

Figure 1. Locations and deformations of embryonic explants extirpated from early gastrula Xenopus laevis embryos. A1, A2: framed areas correspond to the blastocoel roof and suprablastoporal area explants correspondingly. B: non-deformed explant left pricked onto four needles. C: stretching of an explant by shifting one pair of needles. D: shrinkage of explant by bringing needles together.

Figure 2. Different orientations of mutual shifts (solid arrows) of two arbitrarily selected cells (blue and pink). 1 and 2 are the initial and the final distances between cells. Angles between cell trajectories are shown. Middle point inside a cell was used for the distance measurements.

Figure 3. Morphology and cell structure of the blastocoel roof explants. A-C: total views of explants immediately after end of stretching, 30 min and 4 h later respectively. White slits in A are traces of the needles shifts. Heavily pigmented areas in A and B indicate indentations oriented in the stretch direction. Dotted contours in C encircle explants areas which overlap the needles (white holes) in C. D, E: actin stained confocal views of non-stretched explants at the start of incubation (D) and 2 h later. Inset displays surface view of 10-25 min cultivated double blastocoel roof explant. Dashed lines show transitory grooves. E: the arrow points to tangentially contracted cells, dotted contours outline files of extended cells. F-H: similar views of stretched explants, 5, 15 and 60 min after force application.

Figure 4. Vector maps of the outer ectodermal cells shifts in the different kinds of samples during first 15 min after the start of incubation. In this entire diagram, the vertical direction corresponds to the antero-posterior embryo axis, with the posterior pole downwards. A: non-stretched, B: stretched blastocoel roof explants. C: non-stretched, D and E: stretched, F: shrunk SBA explants. Large arrows display needles' shifts. Lengths of vectors are proportional to the rates of cell shifts and are scaled to bars which are 500 μm in A, B and 250 μm in C-F. In the cases of bent vectors, the first part is proportional to the average rates during first 5 min and the second one during 5-15 min. Vectors refer to the active cell displacements.

Figure 5. Rates/angular distributions diagrams of Vm –s in the blastocoel roof (A-C) and suprablastoporal areas (D-F) explants. A, D: non-stretched, B, E: stretched, C, F: shrunk explants. Horizontal axes: converging (negative) and diverging (positive) Vm-s rates (μ/min) during first 5 min after the start of incubation (separated by vertical dashed/dotted line). Vertical axes indicate angles of the mutual shifts of selected cells. Dotted lines correspond to 90^0 value. Figures at each frame top right are the relations of the amounts of angles greater and smaller 90^0.

Figure 6. 2-dimensional maps of the longitudinal (A-D, G-K) and transversal (E, F) components of non-stretched (A, B) and stretched (C-F) BRe and non-stretched (G, H) and stretched (I, K) SBAe. Curved lines display domains borders. Vectors show the directions of cell shifts within each domain. display horizontal components of cell shifts Colors from brown to light green correspond to diminishing of cell shift rates.

Figure 7. Averaged temporal dynamics of detrended distributions of convergent/divergent mutual cell shifts in BRe under different mechanical regimes. Times after start of incubation are shown for each next horizontal row. A-I: non-stretched, B-J: stretched, C, F: shrunk sets of samples.

Horizontal axes: rates of convergent (negative) and divergent (positive) mutual cell shifts, μm/min. Vertical axes: deviations from normal distributions.

Figure 8. Detrended distributions of mutual cell shifts rates for SBAe (A-F) in successive time periods and for intact SBA (G). A, D: non-stretched, B, E: stretched, C, F: shrunk sets of samples. Other designations as in Fig. 7.

Figure 9. Detrended distributions of the mutual cell shifts rates in several arbitrary selected individual non-stretched (upper row) and stretched (lower row) BRe samples. Converging shifts are to the left and diverging shifts to the right of the dashed lines. Note the considerable variability of individual patterns.

Figure 10. Average rates (vertical axes, μm/min) of converging (blue) and diverging (pink) Vm rates in non-stretched (A) and stretched (B) BRe samples during successive time periods from the start of incubation (shown). Note the reversion of converging/diverging rates relations.

Figure 11. Polar diagrams of the rates (μm/min) of directed cell movements in the individual non-stretched BRe samples during successive time periods after start of incubation. Upper row: 0-5 min, lower row: same samples, 5-15 min. Note the angular clustering of cell trajectories and the shifts of the dominating orientations in the course of time.

Figure 12. Histograms of the order function constituents [3 (cosφ)2 – 1] within 0-90^0 range for 8^0 sets of V_d rates. Left column: non-stretched samples, 0^0 coincides with the reduced directions of a maximal trajectories alignment (see text). Middle and right columns: stretched BRe, 0^0 coincides with the directions of force application.

Figure 13. Histograms similar to Fig. 12 for non-stretched (A), stretched (B) and shrunk (C) SBAe) measured in the first 15 min of incubation. AP: antero-posterior, Tr: transversal embryo axis.

Figure 14. Cell rates/angles diagrams for non-stretched (A, D), stretched (B, E) and shrunk (C, F) BRe samples. Upper row: 0-5 min, lower row: 5-15 min times from start of incubation. Horizontal axes: Vd rates, μm/min. Vertical axes: angles. In A, D 0/360^0 angle corresponds to the direction of the main alignment, in B, E to the orientation of stretching force, in C, F it is perpendicular to the direction of shrinkage.

Figure 15. SBAe diagrams of Fig. 14 type. Inset in D is the diagram (scaled to angular axis) for intact SBA.

Figure 16. Bimodality of the directed cell shifts rates as revealed by comparison with detrended normal distributions. Upper row: 0-5 min, bottom row (except G): 5-15 min from the start of

incubation. A, E: stretched BRe; B, F: non stretched SBAe; C: stretched SBAe; G: intact SBA; D, H: shrunk SBAe.

Figure 17. Contraction-extension feedback, as expected by HR model. A: a small contraction of an arbitrary located area (red converging arrows) produces a passive stretching of the resting tissue (blue double-head arrow). B: the active (for example, intercalation-mediated) response of a previously stretched area, overcompensating a preceded stretching (by transforming it into similarly directed pressure, red double-headed arrow) will produce a passive compression of the left area (converging blue arrows). C: overcompensation of a preceding compression of the left area by the next round of active contraction (converged red arrows). Due to tissue incompressibility, the contraction may produce perpendicular extension (double headed blue vertical arrow) which initially is passive but may be later transformed into the active form. After a certain time period all the stress-generating components of the system will come into their active state.

Figure 18. Mechanics of self-focused orthogonal cell flows. Black vertical arrows display forces stretching an explant while black horizontal ones illustrate Poissonian shrinkage. Black spots on the lower side are fixed needles. Dotted lines coming from A to B or to C illustrate longitudinal extension or transversal contraction of representative cell rows. Red double-headed arrows display active extension, red converging arrows indicate active contractions. Blue arrows show these same deformations extending passively. Shadowed double-headed arrows in B are the gradients of passive tension going uphill towards dark areas. Dense orange in B indicates polar areas beyond the needles (cf. Fig. 3). D: a sketch of cell flows moving uphill along tension gradients from relaxed/compressed zones (blue semicircles) towards maximally tensed ones (pink ovals).

Figure 1

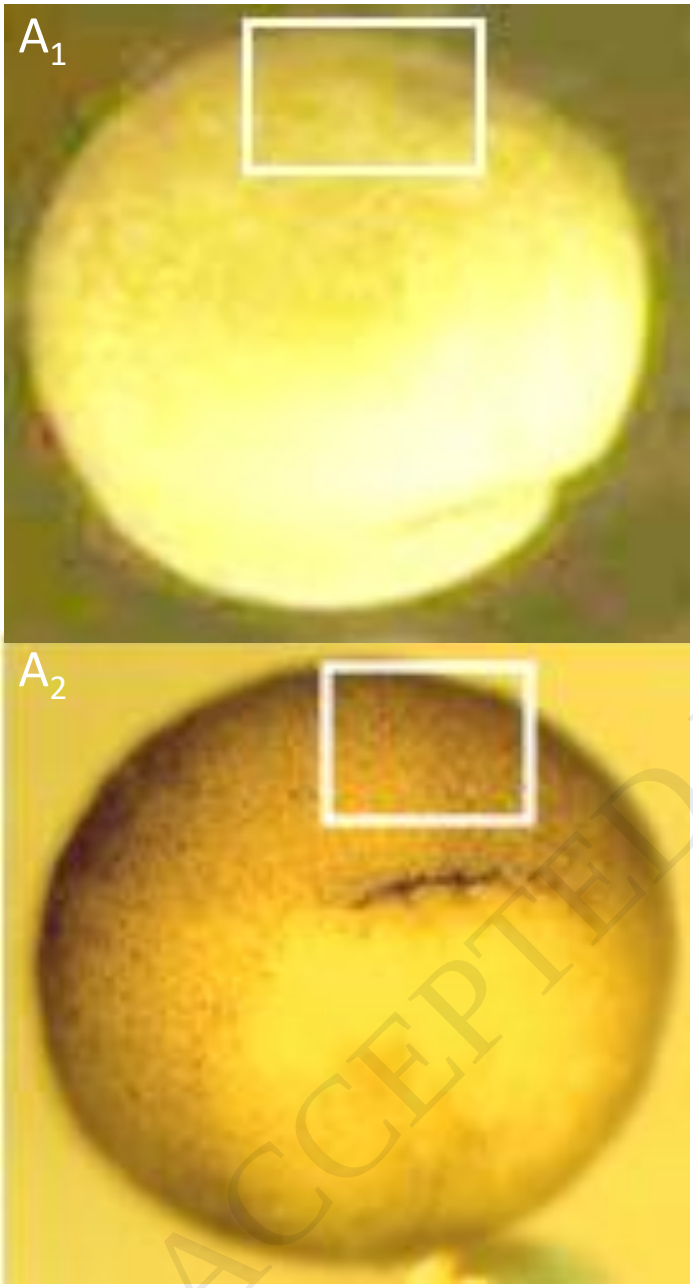

Figure 2

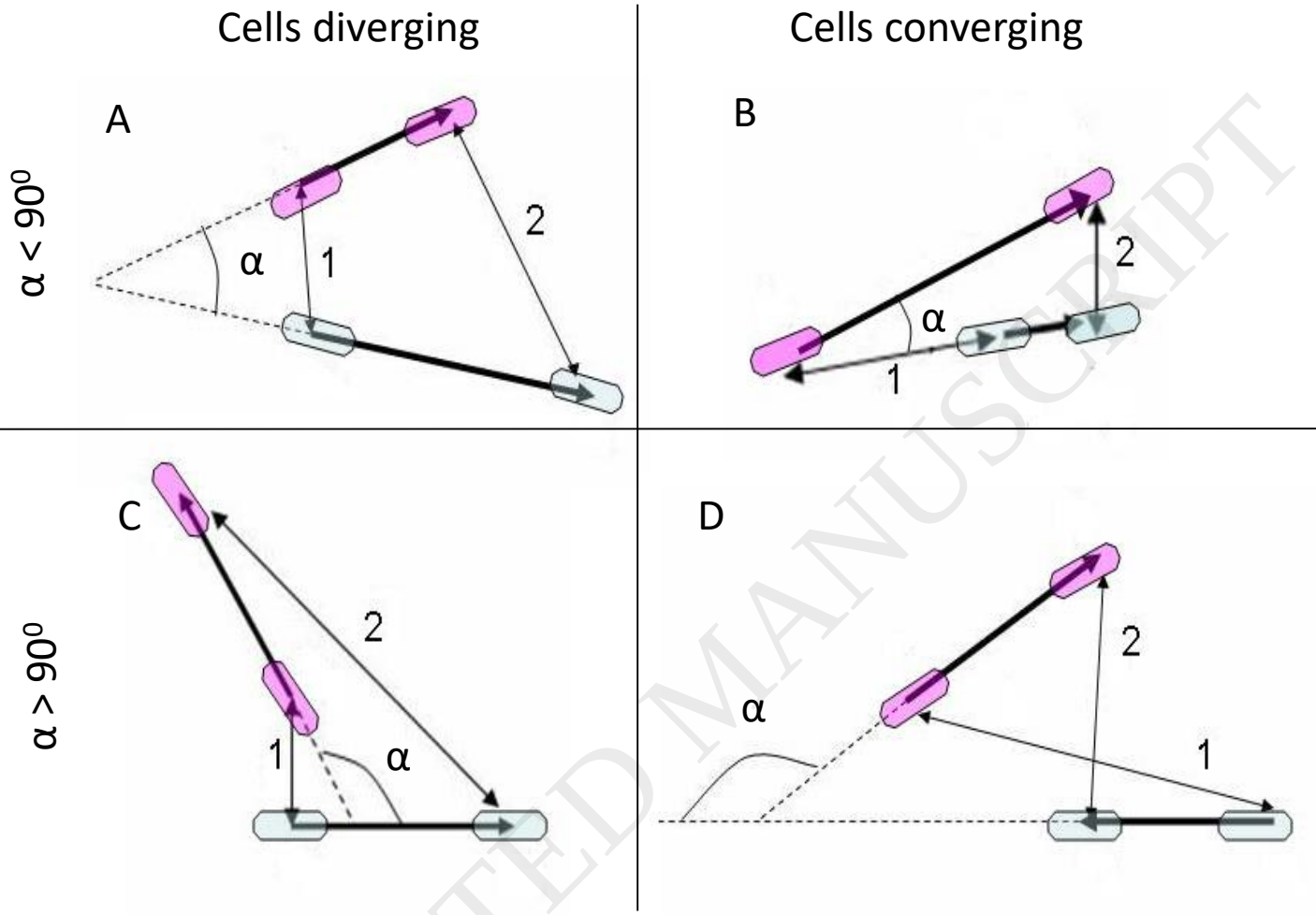

Figure 3

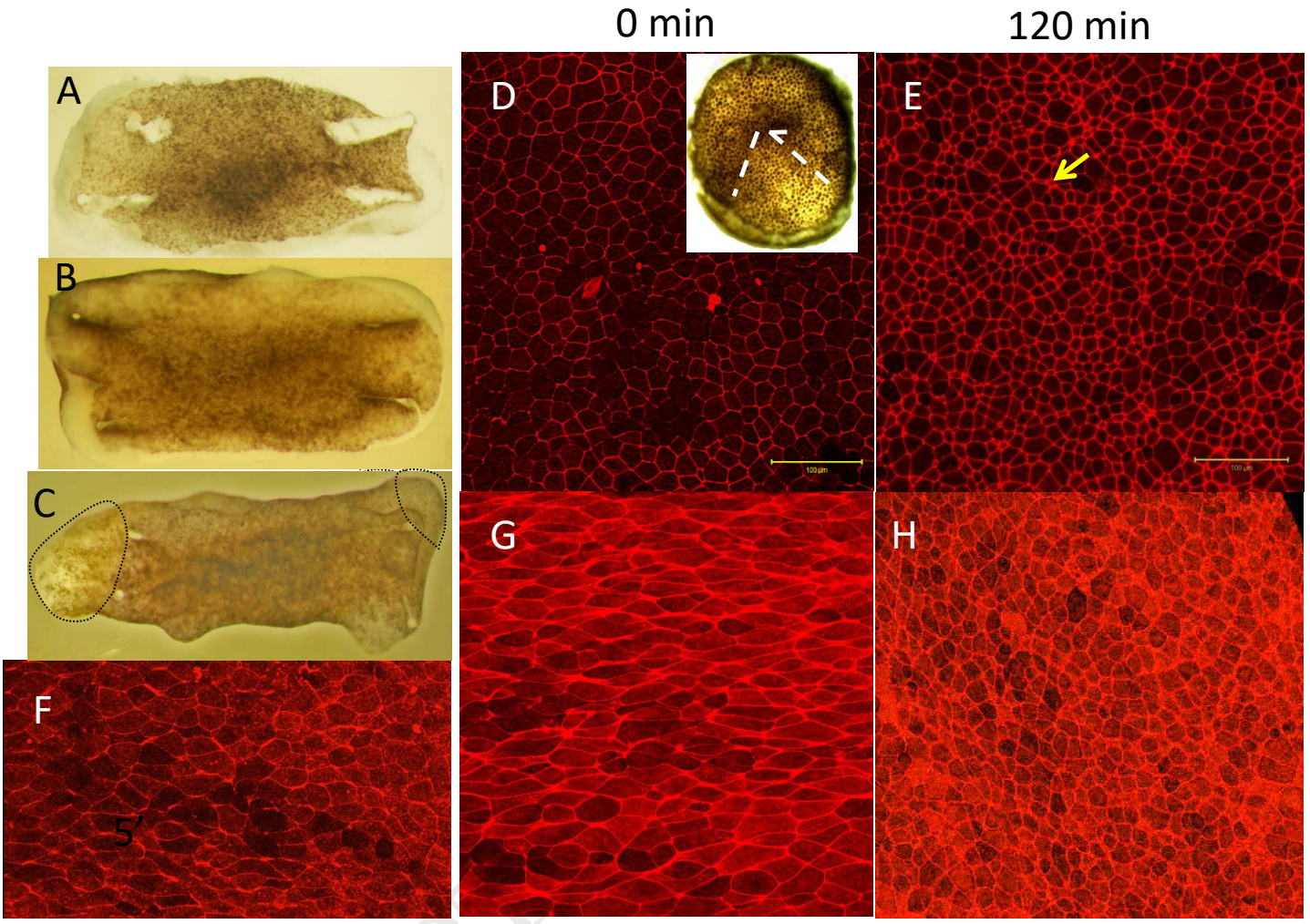

Figure 4

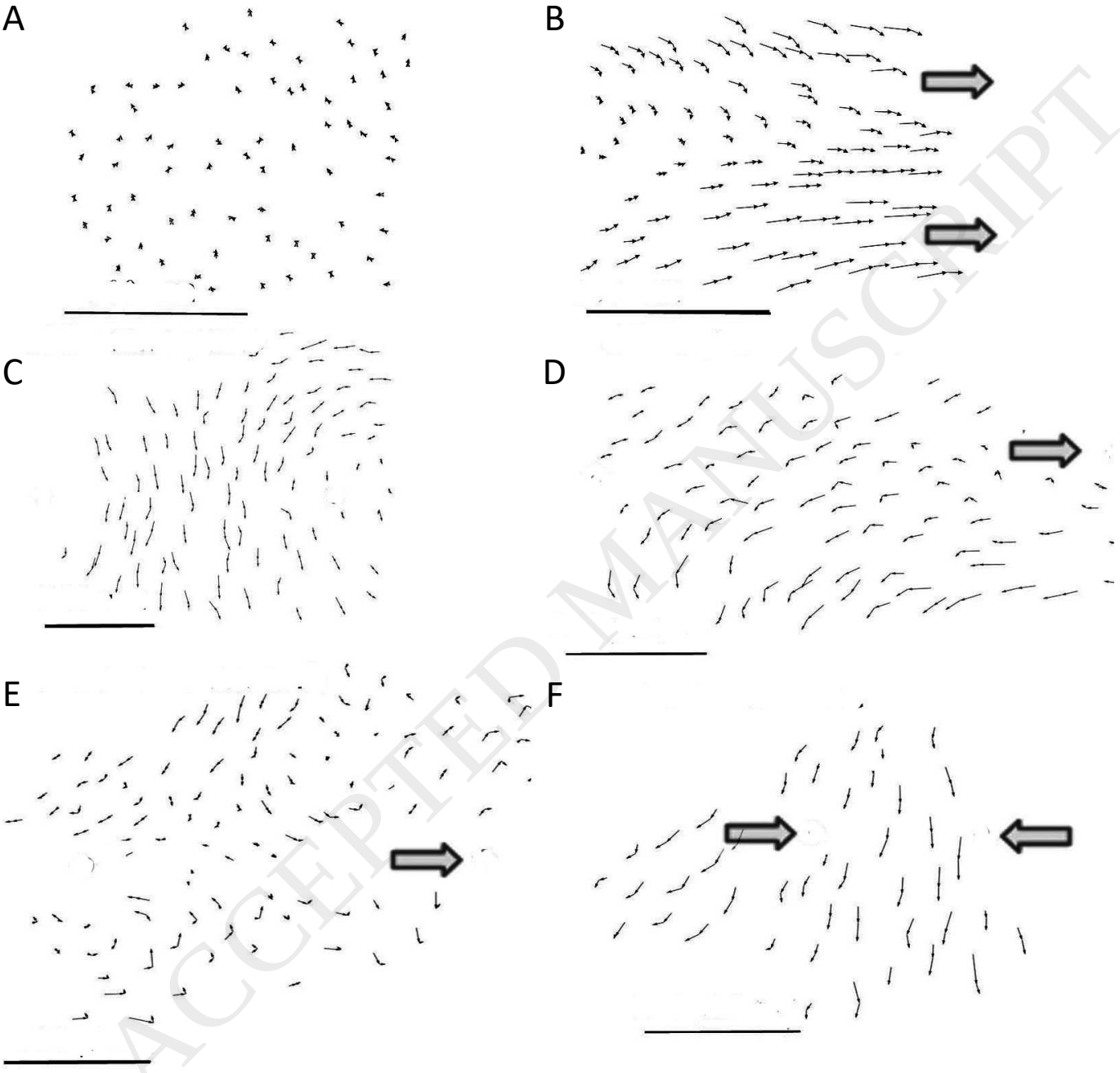

Figure 5

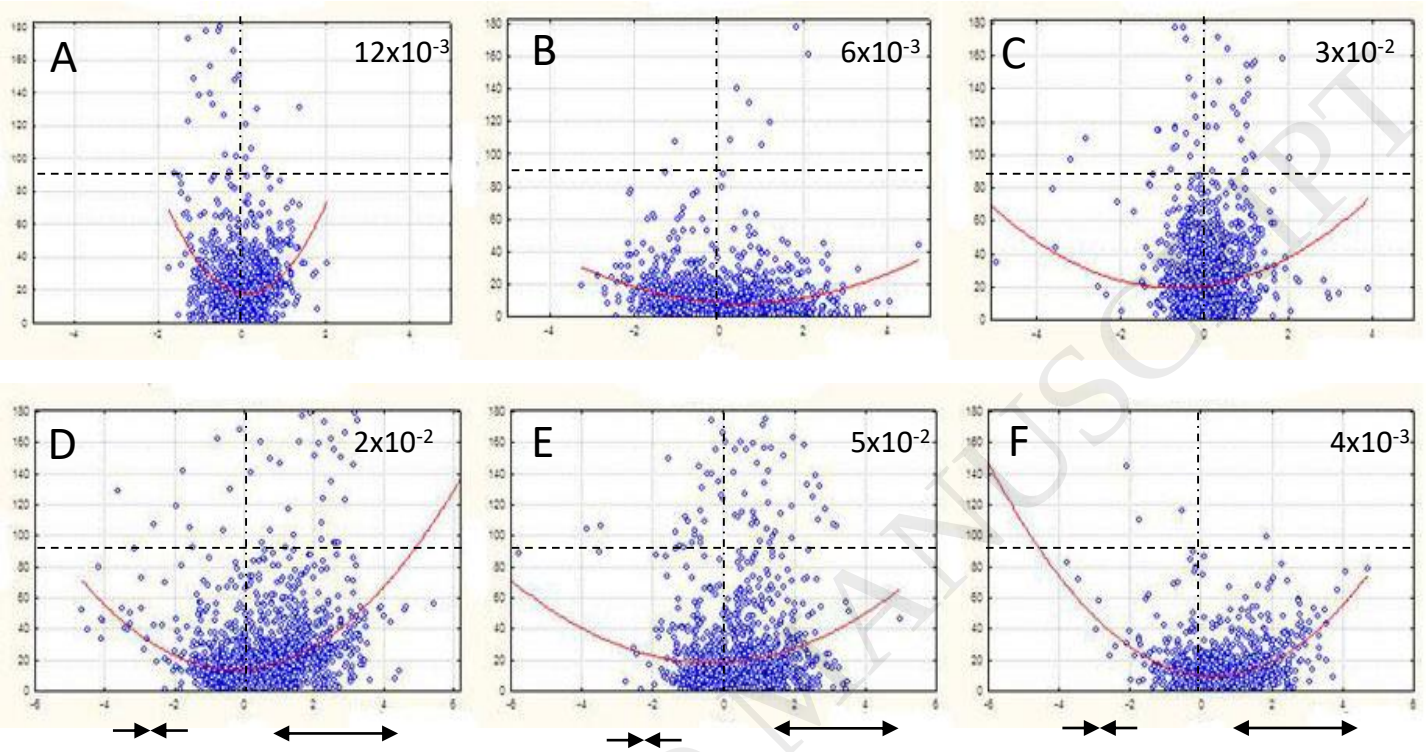

Figure 6

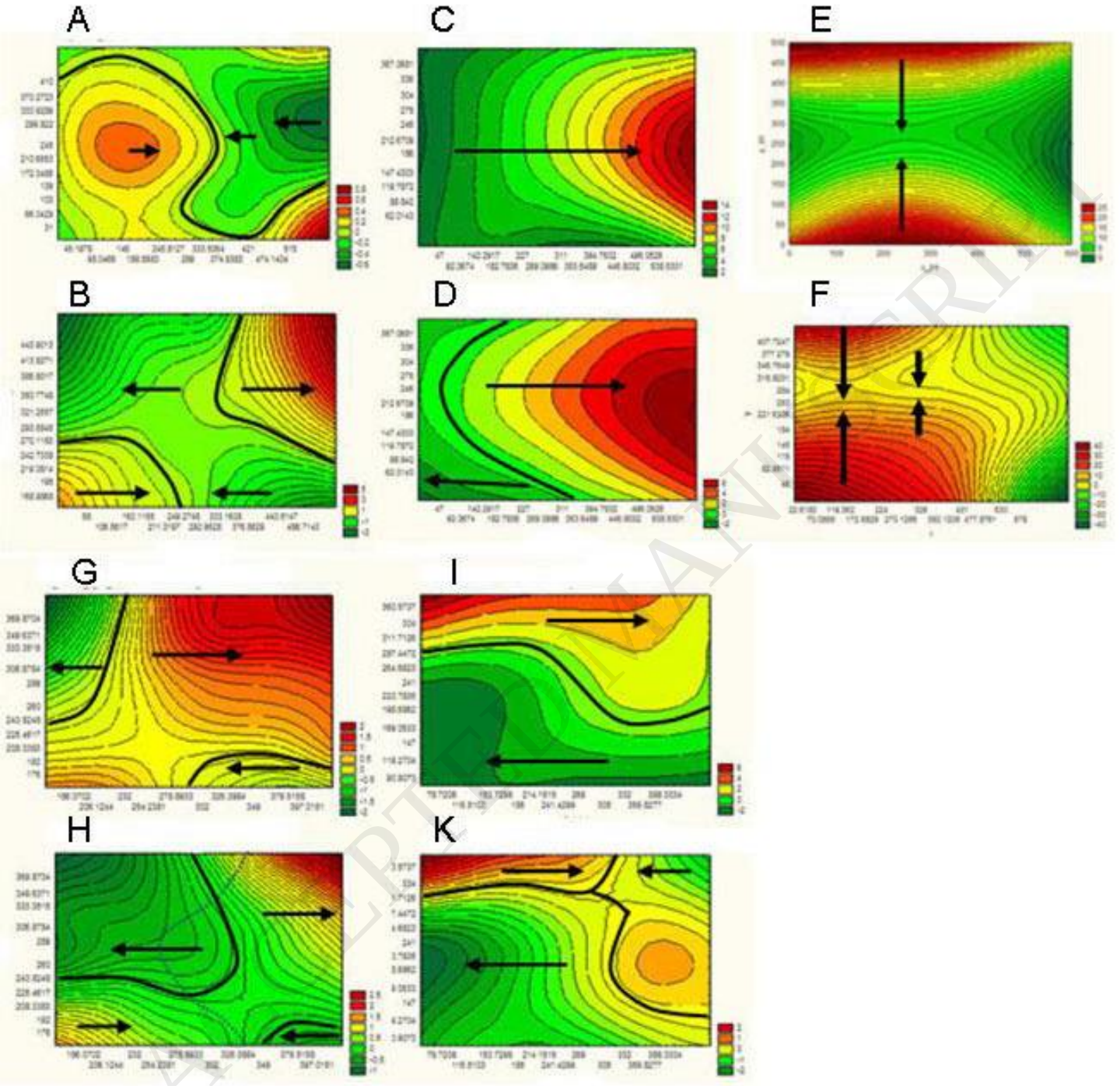

Figure 7

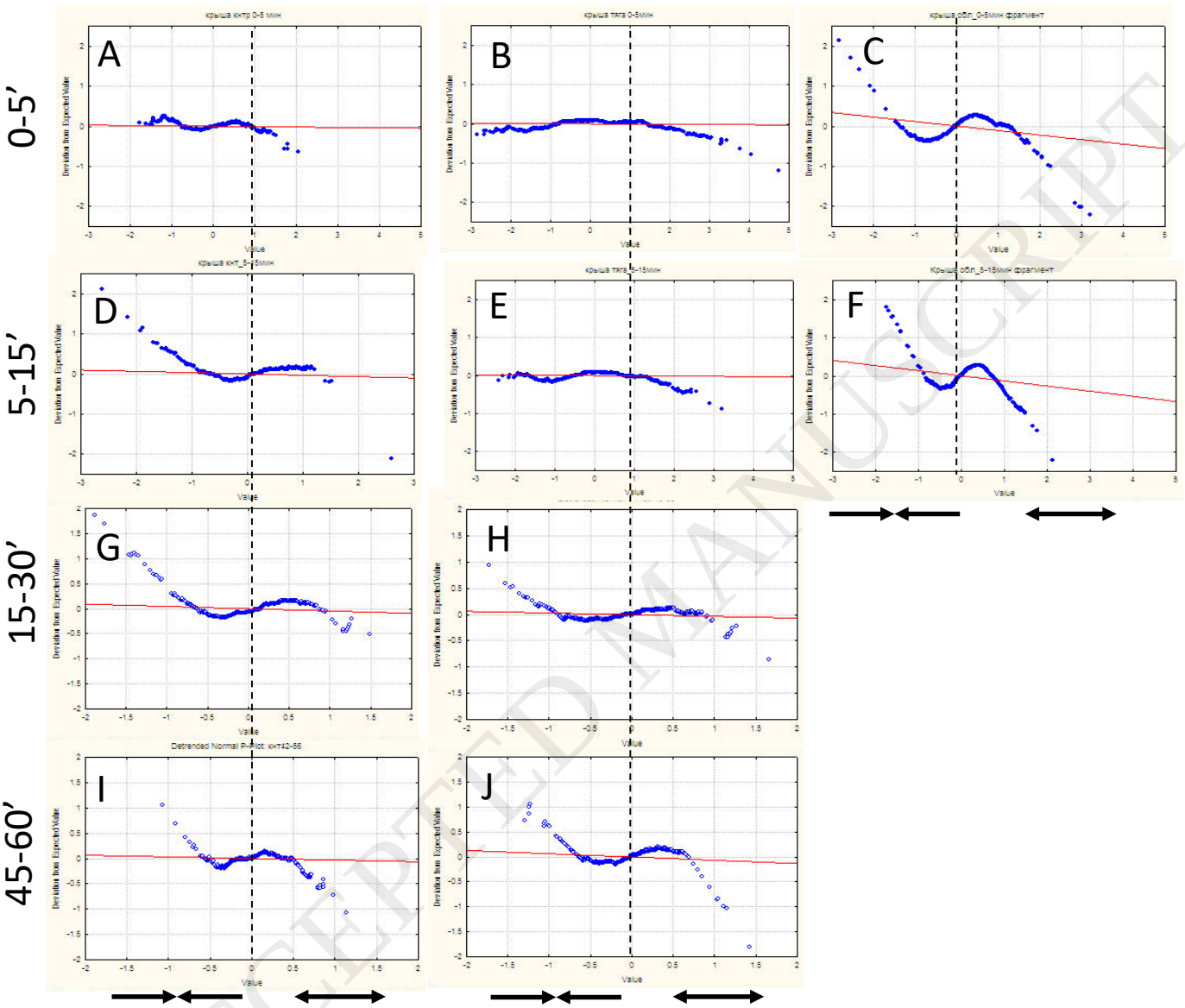

Figure 8

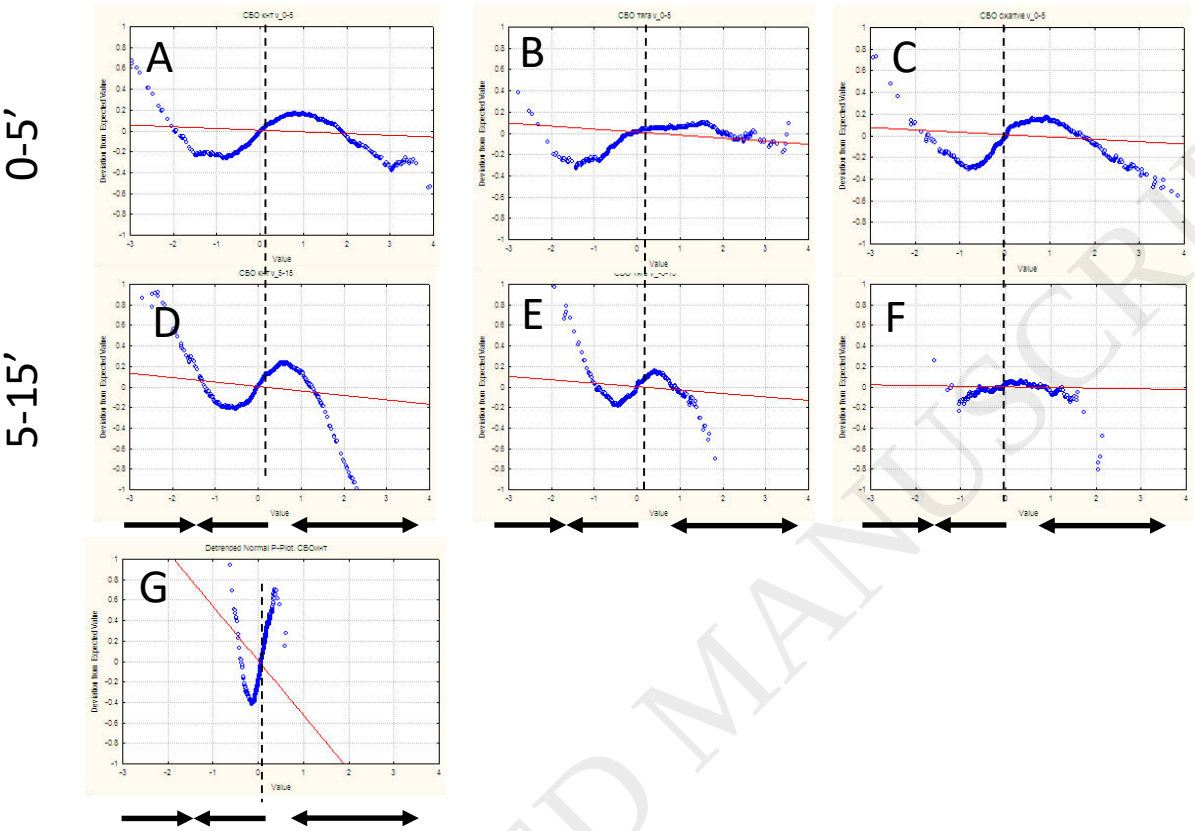

Figure 9

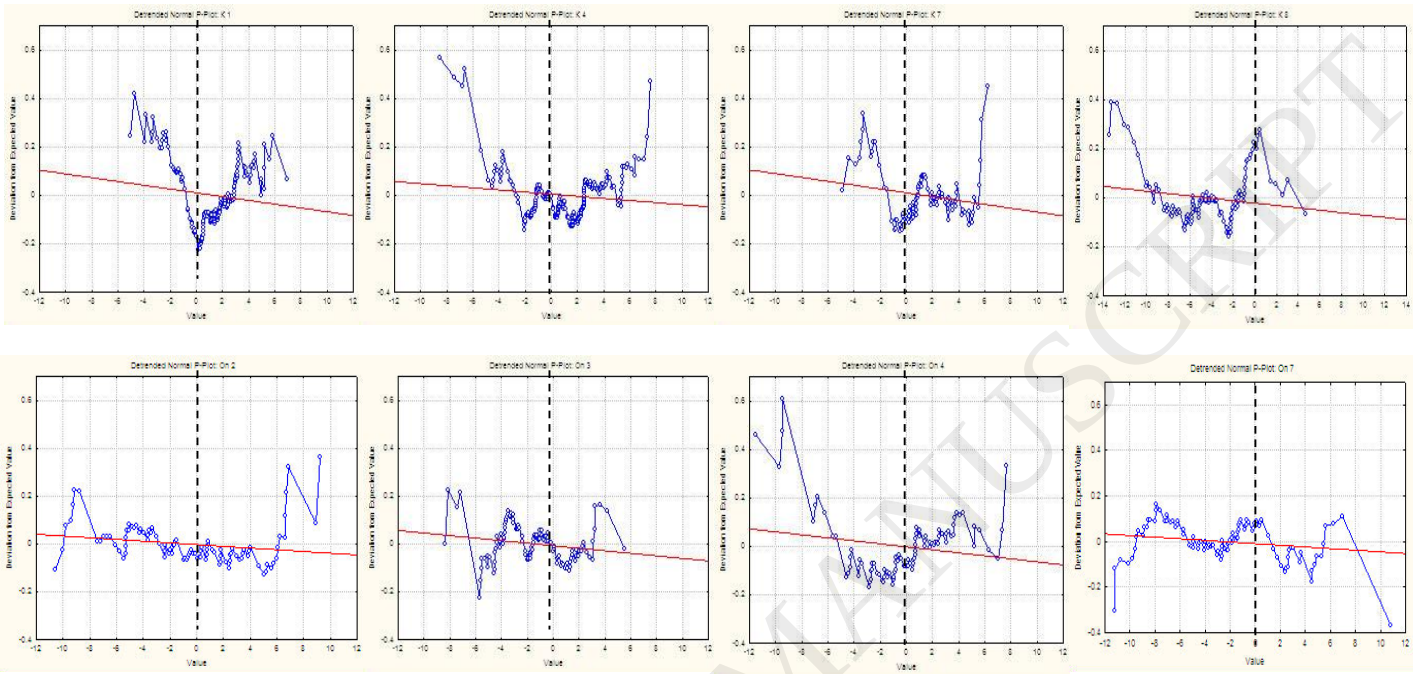

Figure 10

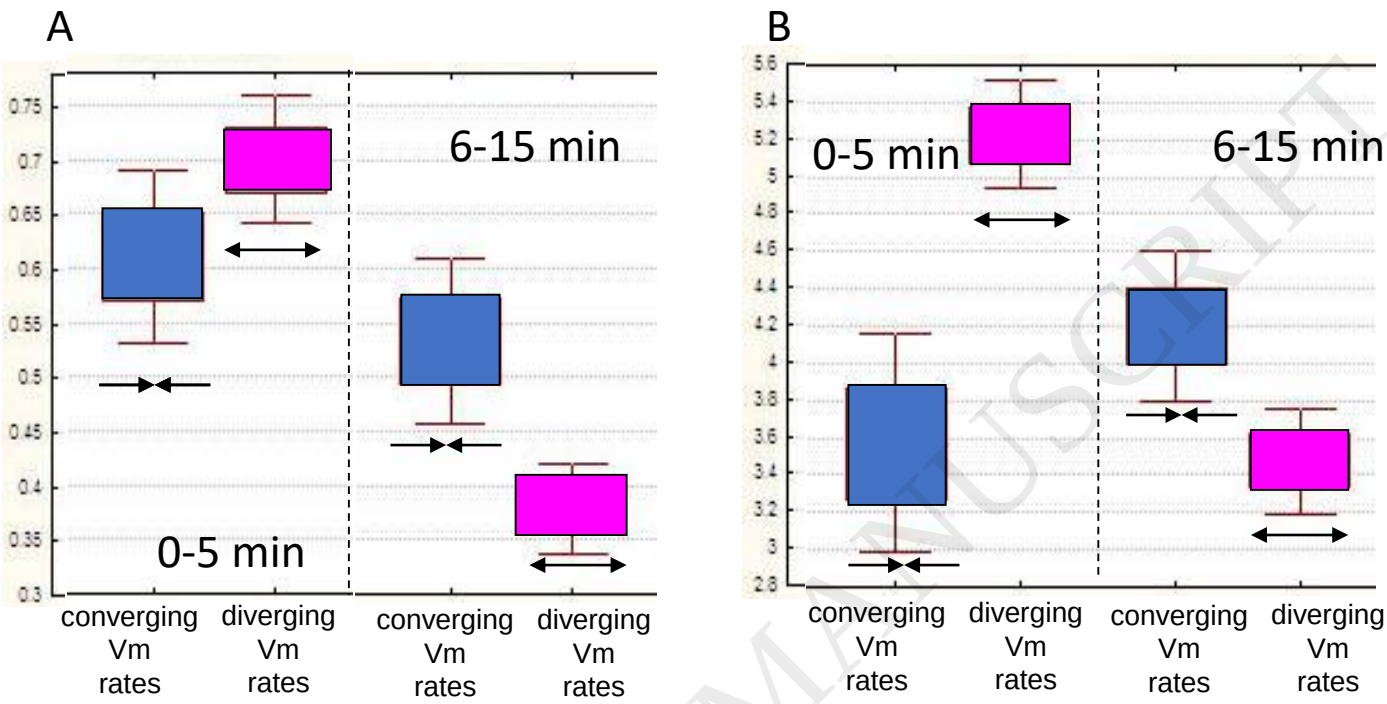

Figure 11

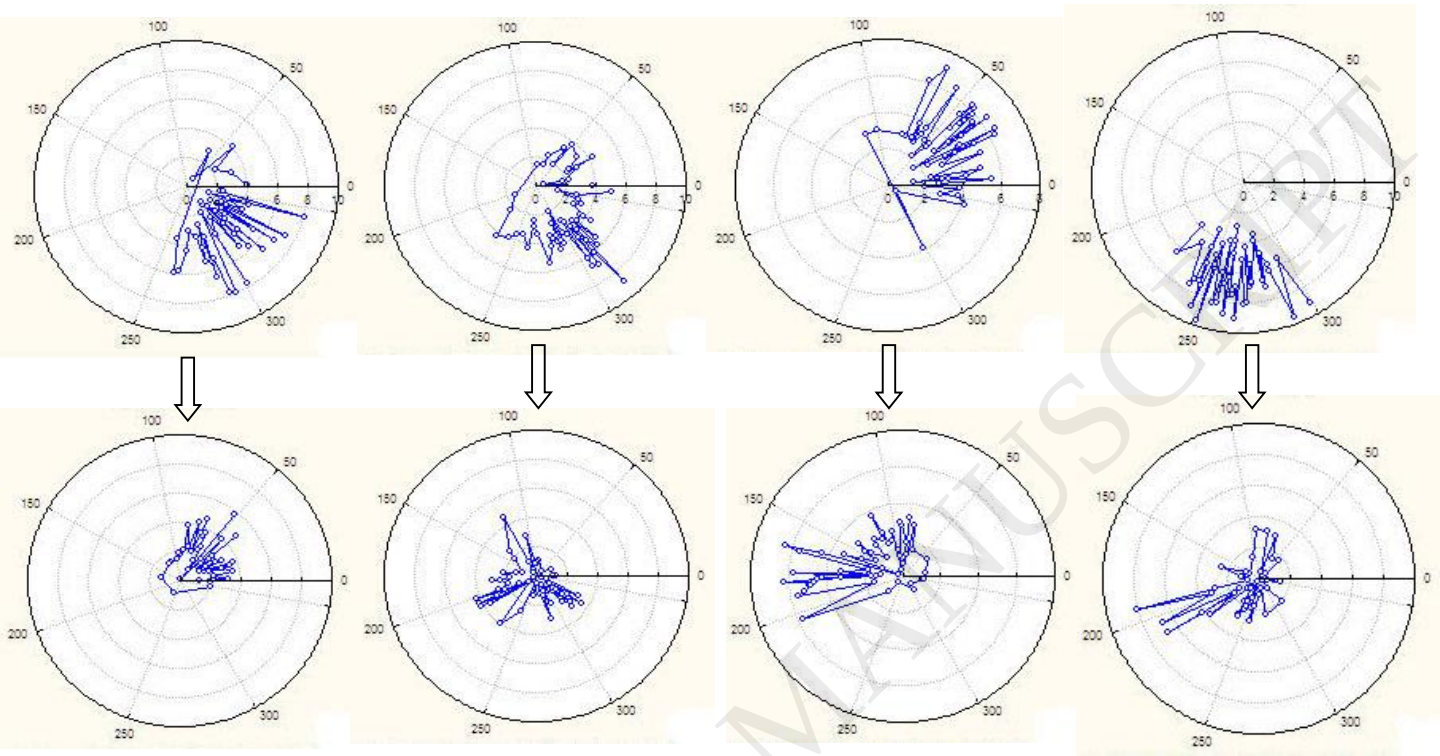

Figure 12

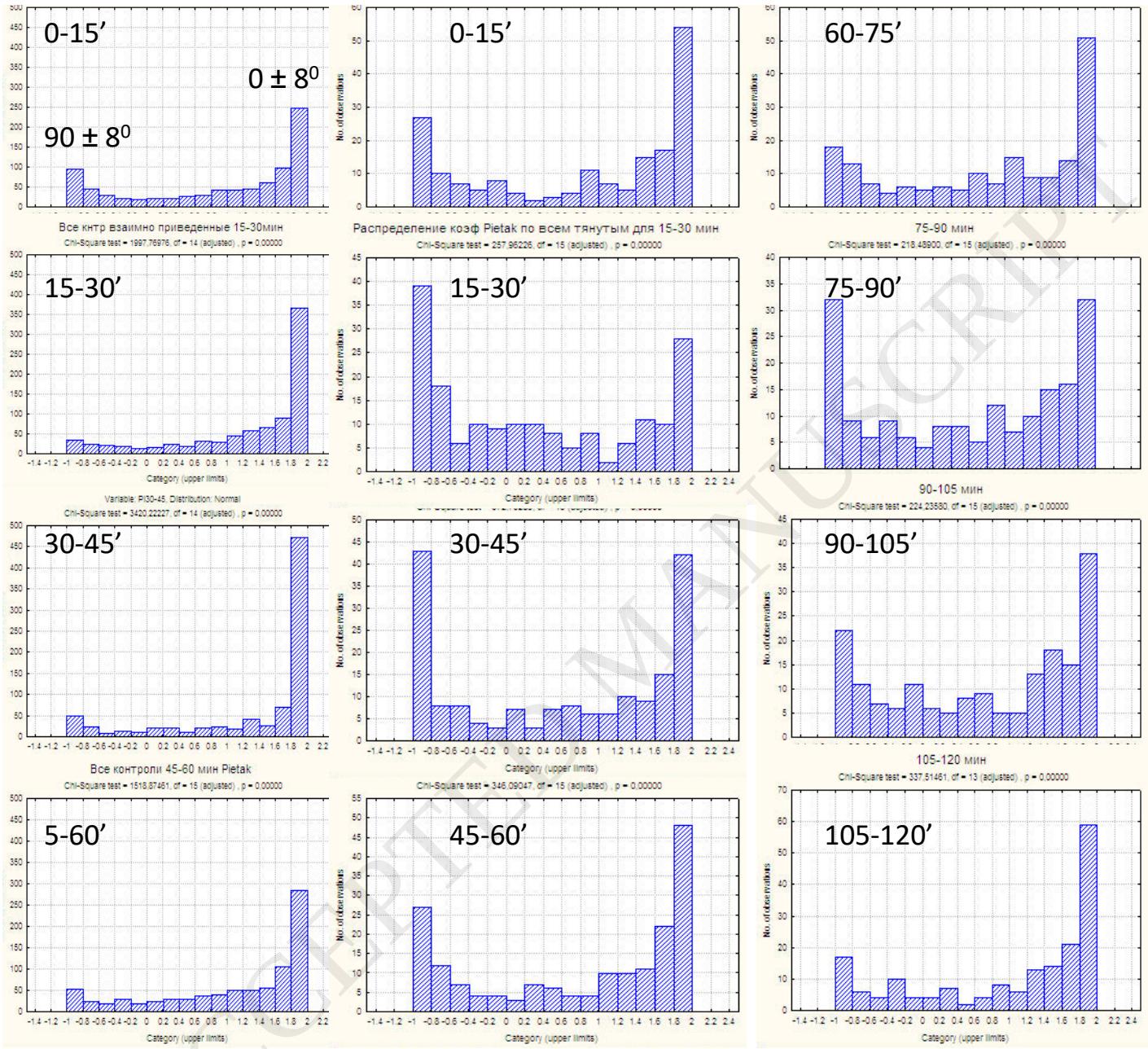

Figure 13

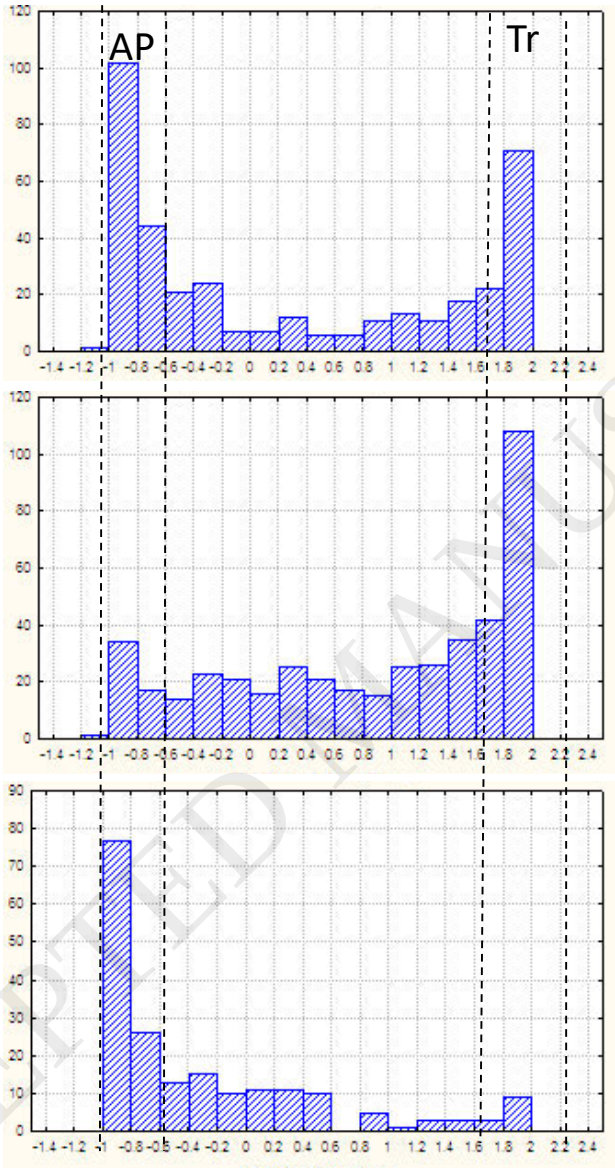

Figure 14

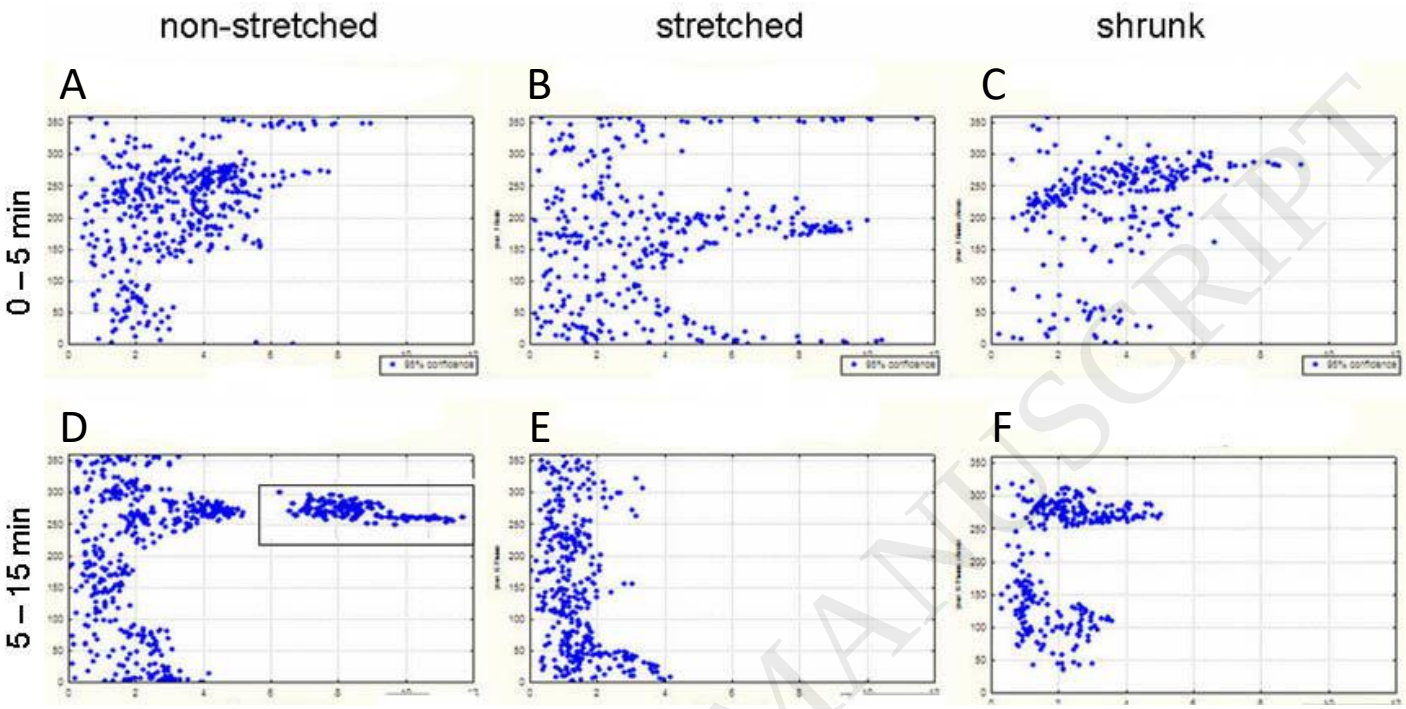

Figure 15

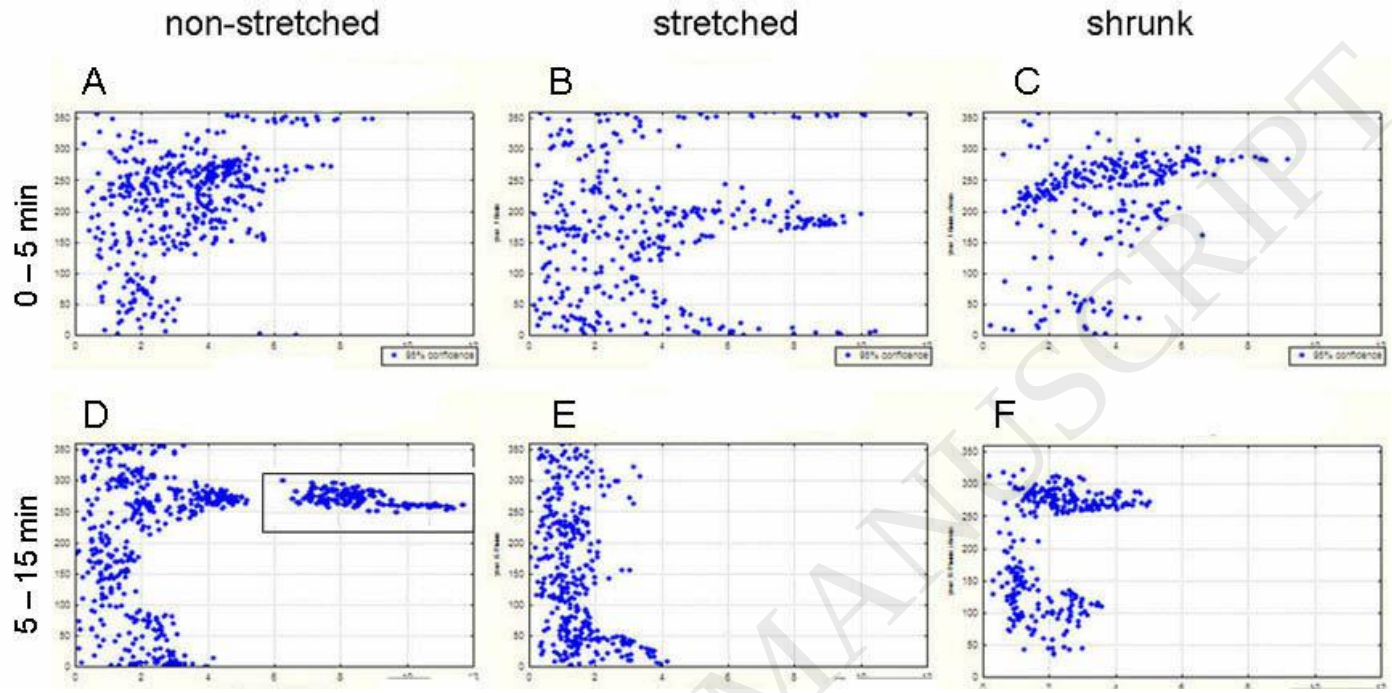

Figure 16

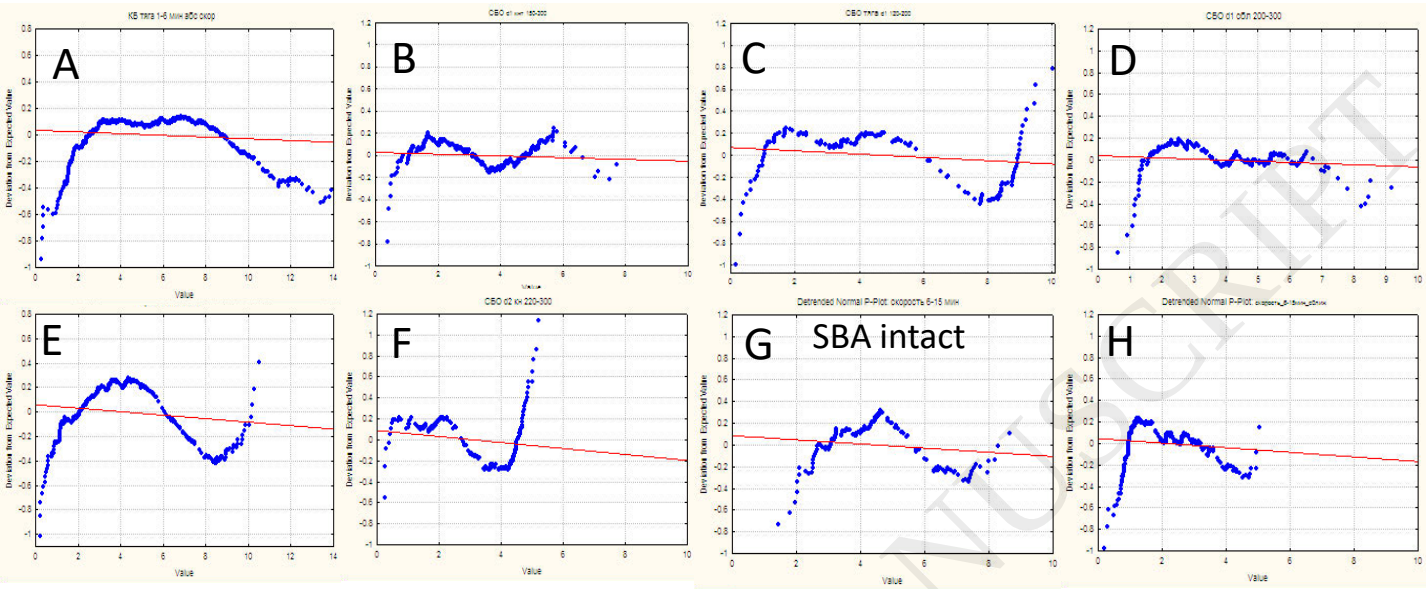

Figure 17

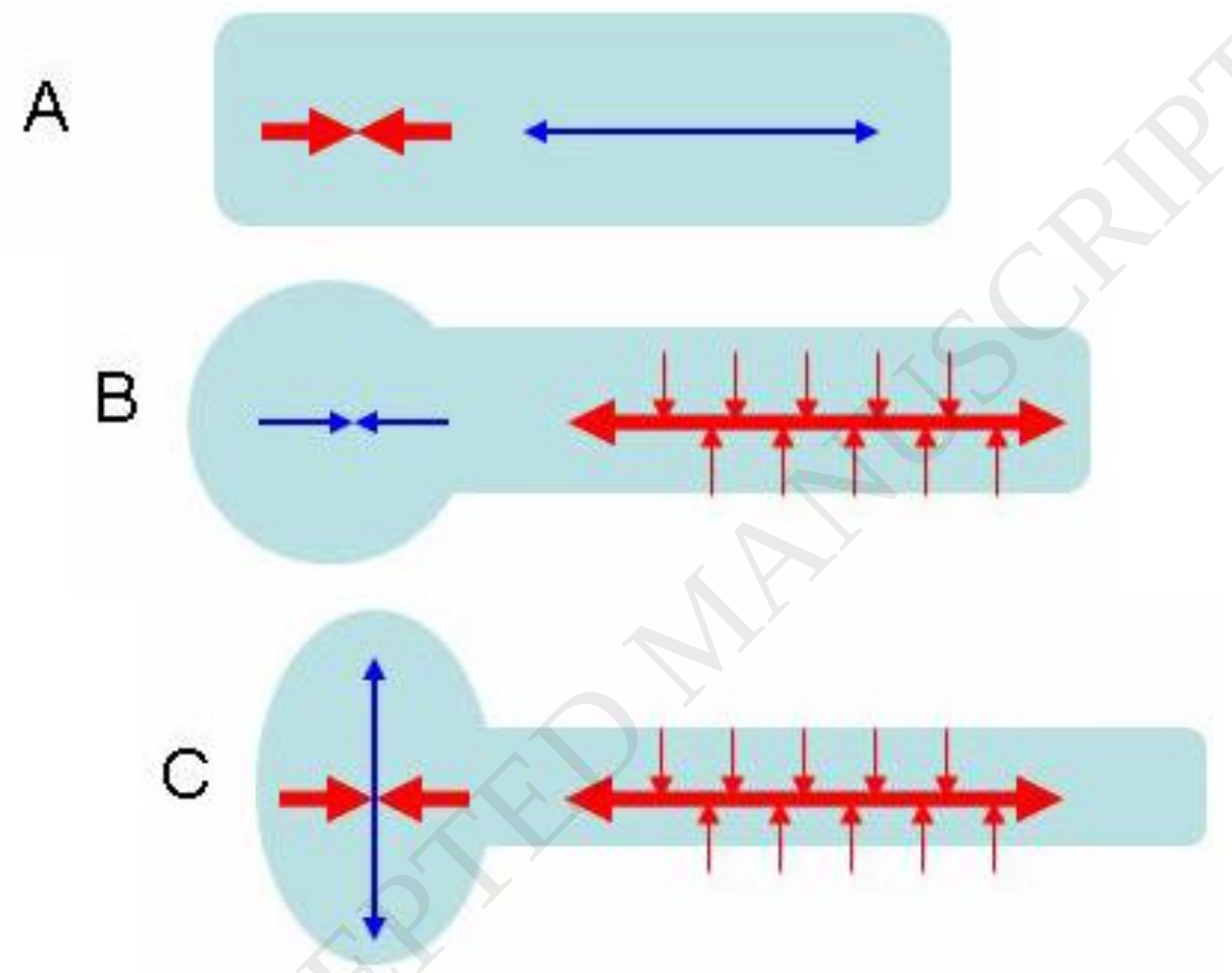

Figure 18

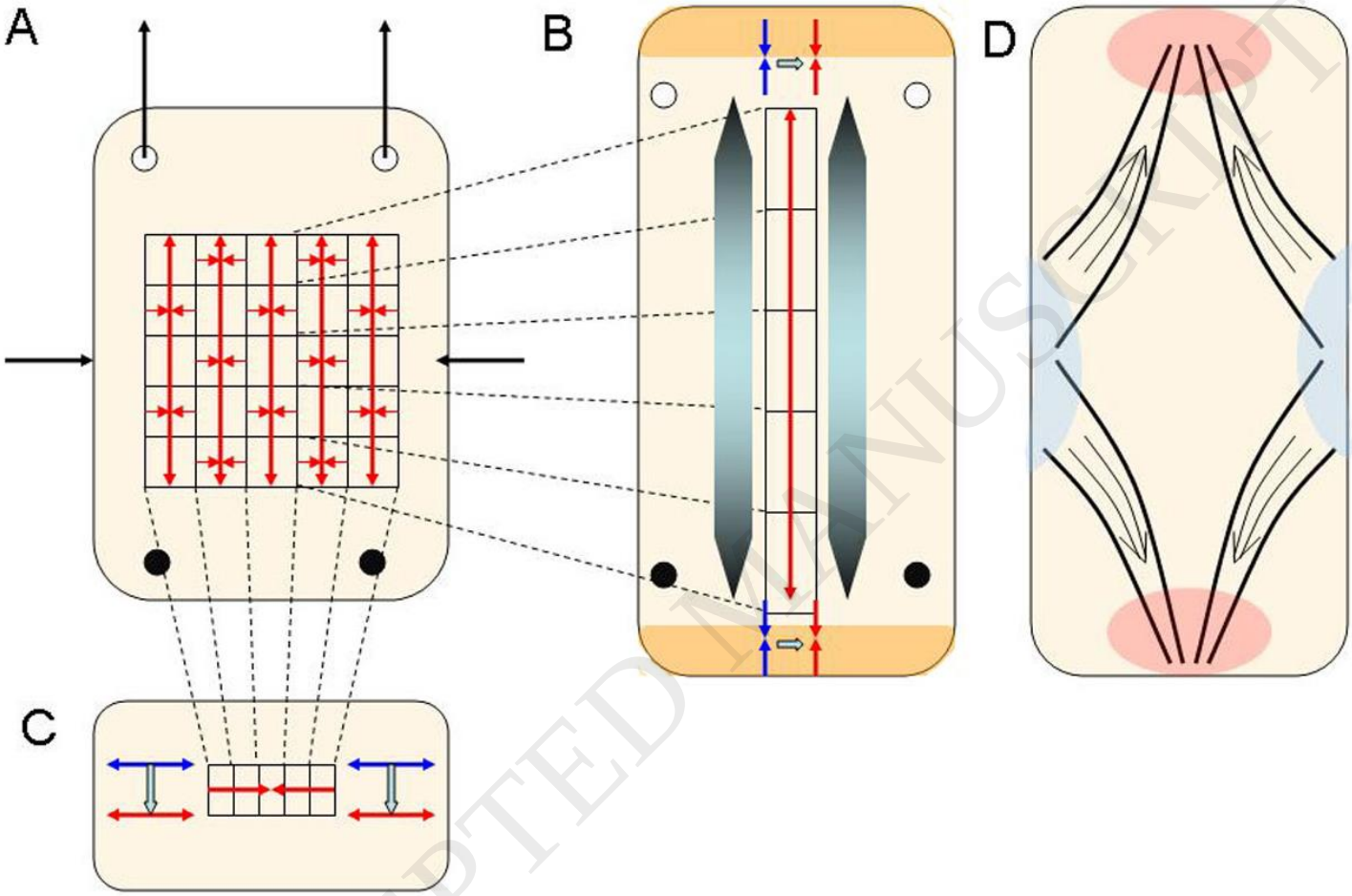

Table 1. Average rates and trajectories angles of diverging and converging V_m components. Numbers of measurements are shown in brackets.

Samples	V_m components, average values		Average angles of V_m trajectories
	diverging	converging	
BR non-stretched	0,13 ± 0,11 (577)	0,12 ± 0,10 (476)	20,8 ± 20,5
BR stretched	0,31 ± 0,24 (642)	0,25 ± 0,19 (709)	10,6 ± 14,9
BR shrunk	0,14 ± 0,14 (862)	0,12 ± 0,15 (774)	20,7 ± 24,4
SBA non-stretched	0,33 ± 0,28 (1416)	0,20 ± 0,22 (712)	18,8 ± 23,3
SBA stretched	0,32 ± 0,24 (882)	0,21 ± 0,25 (494)	21,1 ± 30,0
SBA shrunk	0,33 ± 0,26 (804)	0,19 ± 0,22 (286)	13,2 ± 16,3
SBA intact	0,12 ± 0,09 (578)	0,15 ± 0,22 (368)	3,1 ± 2,6

Table 2. Correlation coefficients between the numbers of cells moving within15^0 angular sectors and their average rates. For all the groups correlation coefficients are significant ($p > 0,95$).

Samples categories	r (N/ V_d)
SBA control	+ 0,84
SBA stretched	+ 0.83
SBA shrunk	+ 0,87
BRs control	+ 0,58
BRs stretched	+ 0, 86
BRs shrunk	+ 0,53